EFFECT OF TRANSVERSE ISOTROPY ON TENSILE STRENGTH AND DEFORMABILITY OF SANDSTONE

SAWAROT SUWANKEEREE

A Thesis Submitted in Partial Fulfillment of the Requirement for the
Degree of Master of Philosophy of Engineering in Civil, Transportation
and Geo-Resources Engineering
Suranaree University of Technology
Academic Year 2021

ผลกระทบของทรานซ์เวอร์สไอโซทรอปีต่อกำลังดึงและการเปลี่ยนแปลงรูปร่างของหินทราย

นางสาวสวรส สุวรรณคีรี

วิทยานิพนธ์นี้เป็นส่วนหนึ่งของการศึกษาตามหลักสูตรปริญญาวิศวกรรมศาสตรมหาบัณฑิต
สาขาวิชาวิศวกรรมโยธา ขนส่ง และทรัพยากรธรณี
มหาวิทยาลัยเทคโนโลยีสุรนารี
ปีการศึกษา 2564

EFFECT OF TRANSVERSE ISOTROPY ON TENSILE STRENGTH AND DEFORMABILITY OF SANDSTONE

Suranaree University of Technology has approved this thesis submitted in partial fulfillment of the requirements for a Master's Degree.

Thesis Examining Committee

_____

(Assoc. Prof. Dr. Pornkasem Jongpradish)

Chairperson

_____

(Dr. Thanittha Thongprapha)

Member (Thesis Advisor)

_____

(Asst. Prof. Dr. Prachya Tepnarong)

Member

_____

(Prof. Dr. Kittitep Fuenkajorn)

Member

_____   _____

(Assoc. Prof. Dr. Chatchai Jothityangkoon)   (Assoc. Prof. Dr. Pornsiri Jongkol)

Vice Rector for Academic Affairs   Dean of Institute of Engineering

and Quality Assurance

สวรส สุวรรณคีรี : ผลกระทบของทรานซ์เวอร์สไอโซทรอปีต่อกำลังดึงและการเปลี่ยนแปลง
รูปร่างของหินทราย (EFFECT OF TRANSVERSE ISOTROPY ON TENSILE STRENGTH
AND DEFORMABILITY OF SANDSTONE) อาจารย์ที่ปรึกษา : ดร.ธนิษฐา ทองประภา,
69 หน้า.

คำสำคัญ: ระนาบชั้นหิน/หมวดหินภูพาน/การทดสอบแรงดึงแบบบราซิล/สัมประสิทธิ์ความยืดหยุ่น/
อัตราส่วนของปัวซอง

การศึกษานี้มุ่งผลกระทบของทรานซ์เวอร์สไอโซทรอปีต่อกำลังรับแรงดึงและสัมประสิทธิ์
ความยืดหยุ่นของหินทรายหมวดหินภูพานภายใต้การทดสอบแรงดึงของบราซิล แผ่นตัวอย่างหิน
มีขนาดเส้นผ่าศูนย์กลางเท่ากับ 74 มิลลิเมตร และหนา 37 มิลลิเมตร การทดสอบดำเนินการภายใต้
สภาวะความเค้นสองแบบ: (1) ทิศทางความเค้นแบบแกนเดียวและ (2) สภาวะความเค้นแบบสองแกน
ที่มีระนาบชั้นหินตั้งฉากและขนานกับแกนหลัก ผลการทดสอบระบุว่ากำลังรับแรงมีค่าสูงสุด
เมื่อระนาบชั้นหินตั้งฉากกับแนวแรงกดและลดลงจนมีค่าต่ำสุดเมื่อระนาบชั้นหินขนานกับแนวแรงกด
ค่าสัมประสิทธิ์ความหยืดหยุ่นและอัตราส่วนปัวซองได้ถูกคำนวณบนพื้นฐานของสมการทรานเวอร์สลี
ไอโซโทรปิกที่นำเสนอโดยกฎของฮุค ค่าสัมประสิทธิ์ความยืดหยุ่นแบบดึงมีค่าต่ำกว่าค่าสัมประสิทธิ์
ความยืดหยุ่นแบบกด กำลังรับแรงดึงที่ได้จากการจำลองเชิงตัวเลขแสดงแนวโน้มที่ใกล้เคียง
กับผลทดสอบจากห้องปฏิบัติการ การค้นพบนี้สามารถใช้เพื่อประเมินเสถียรภาพของอุโมงค์และ
การขุดใต้ดินของหินทรายภายใต้การวางตัวของระนาบชั้นหินที่แตกต่างกัน

สาขาวิชา เทคโนโลยีธรณี   ลายมือชื่อนักศึกษา สวรส สุวรรณคีรี
ปีการศึกษา 2564   ลายมือชื่ออาจารย์ที่ปรึกษา

SAWAROT SUWANKEEREE : EFFECT OF TRANSVERSE ISOTROPY ON TENSILE
STRENGTH AND DEFORMABILITY OF SANDSTONE. THESIS ADVISOR :
THANITTHA THONGPRAPHA, PhD., 69 PP.

Keyword: Bedding/Phu Phan Formation/Brazilian Test/Elastic Modulus/Poisson' Ratio

This study aims at investigating the effect of transverse isotropy on tensile strength and elastic modulus of Phu Phan sandstone under Brazilian tension test. The disk specimens have 74 mm in nominal diameter and 37 mm in thickness. The tests are performed under two stress states: (1) uniaxial stress direction and (2) biaxial stress state with bedding planes normal and parallel to the core axis. The test results indicate that strengths are largest when bedding planes are normal to loading diameter. They gradually decrease to the smallest value when the beds are parallel to the loading direction. The elastic moduli and Poisson's ratios are calculated based on the transversely isotropic solutions proposed by Hooke's law. The tensile elastic moduli are lower than the compressive elastic moduli. Tensile strengths obtained by numerical simulation show similar trend with the laboratory results. The findings obtained here can be used to assess the stability of tunnel and underground excavations in the sandstone under various orientations of bedding planes.

School of Geotechnology   Student's Signature
Academic year 2021   Advisor's Signature

ACKNOWLEDGEMENTS

Sawarot Suwankeeree

TABLE OF CONTENTS

TABLE OF CONTENTS (Continued)

LIST OF TABLES

LIST OF FIGURES

LIST OF FIGURES (Continued)

LIST OF FIGURES (Continued)

LIST OF FIGURES (Continued)

SYMBOLS AND ABBREVIATIONS

P	=	Load
D	=	Disk diameter
t	=	Disk thickness
R	=	Radial disk
σ_B	=	Brazilian tensile strength
σ_r	=	Radial stresses
σ_θ	=	Tangential stresses
σ_x	=	Stress in x-direction
σ_y	=	Stress in y-direction
σ_c	=	Compression stress
σ_t	=	Tension stress
ε_r	=	Strain in radial stresses
ε_θ	=	Strain in tangential stresses
ε_x	=	Strain in x-direction
ε_y	=	Strain in y-direction
ε_c	=	Compression strain
ε_t	=	Tension strain
θ	=	Angle making with x-axis
β	=	Bedding plane angles
E_{CP}	=	Compressive elastic modulus with beds parallel to loading
E_{CN}	=	Compressive elastic modulus with beds normal to loading
$E_{C(\beta)}$	=	Compressive elastic modulus with angle (β)
E_{TP}	=	Tensile elastic modulus with beds parallel to loading
E_{TN}	=	Tensile elastic modulus with beds normal to loading
$E_{T(\beta)}$	=	Tensile elastic modulus with angle (β)
$\nu_{c(\beta)}$	=	Poisson's ratio of compassion with angle (β)
$\nu_{t(\beta)}$	=	Poisson's ratio of tension with angle (β)
G	=	Shear modulus

CHAPTER I
INTRODUCTION

1.1 Background and rationale

Tensile strength of rock is one of the important parameters for the design of tunnels and underground excavation. The rock tensile strength controls the maximum internal pressure of unlined storage caverns, the maximum roof span of underground openings, and the borehole pressure for hydraulic fracturing (Fuenkajorn and Klanphumeesri, 2010). Tensile strength is usually obtained from Brazilian tension test due to the simplicity of sample preparation and test procedure.

The bedded sedimentary rocks are common widely distributed in civil and geological engineering works, which these rocks are characteristic of discontinuity and anisotropic. Anisotropic behavior affects the stability of tunnel and underground excavation. Many researchers have been performed to study the effect of anisotropy on rock strength under compression. The effect of bedding plane orientations on tensile strength and deformation under tension of rock has rarely been investigated.

1.2 Research objectives

This study aims to determine tensile strength and elastic parameters of transversely isotropic on Phu Phan sandstone. The tasks involve performing Brazilian tension tests under two stress states: (1) uniaxial stress state with bedding planes normal and parallel to the core axis and (2) biaxial stress state with bedding planes normal and parallel to the core axis, calculating the elastic modulus and Poisson's rations under compression and tension with various bedding plane orientations. The numerical simulations can describe the stress distributions and displacement vector under various bedding orientations.

1.3 Scope and limitations

The scope and limitations of the research include as follows.

1) The collected rock specimens belong to Phu Phan sandstone formation obtained from Khorat group.

2) The nominal diameter is 74 mm with 37 mm in length.

3) The inclination angle varied from 0 to 90 degrees.

4) Brazilian tension tests are performed under dry conditions.

5) All tests are conducted at room temperature.

6) The test procedures follow relevant ASTM standard practices (ASTM D3967), as much as practical.

7) The research findings are published in conference papers or journals.

1.4   Research methodology

The research methodology shown in Figure 1.1 comprises 6 steps; including literature review, samples collection and preparation, Brazilian tension test under uniaxial stress and biaxial stress state, analysis of test results, numerical simulations, discussions and conclusions, and thesis writing.
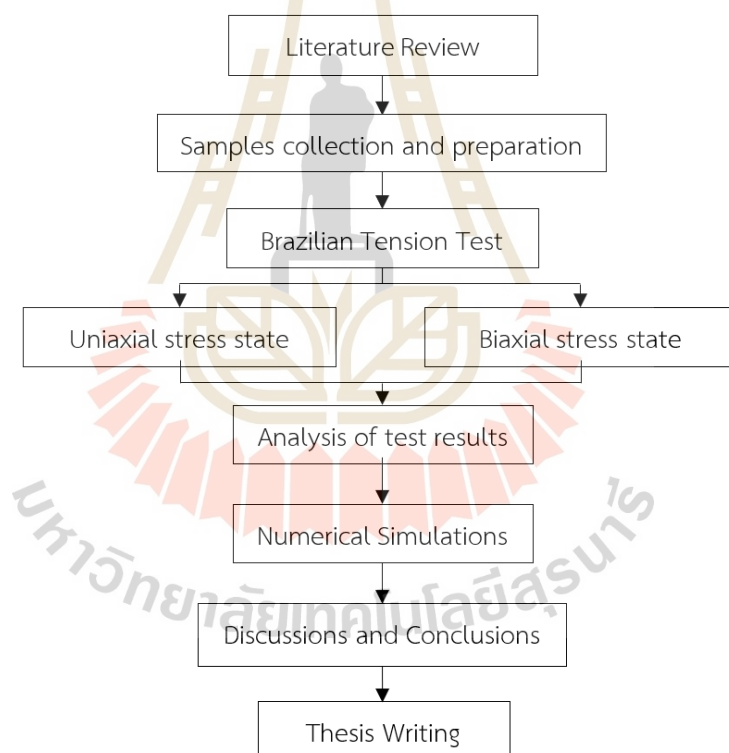
Figure 1.1 Research methodology.

1.4.1   Literature review

A literature review will be performed to study research about the effects of transverse isotropic on tensile strength, the effect of transverse isotropic on elastic parameters, degree of anisotropy, and numerical simulations under Brazilian

tension test. The sources of information are conference, papers journals, and technical reports. A summary of the literature review is given in the thesis.

1.4.2 Samples collection and preparation

Samples used in this study are prepared from Phu Phan sandstone. They belong to the Khorat group which is widely exposed in Northeastern Thailand. The specimens have nominal diameters, (D) of 74 mm with thickness, (t) of 37 mm, prepared with bedding planes parallel and normal to the core axis. The selection criteria for this sandstone are the availability and well-defined bedding planes. A total of 22 samples are prepared. The sandstone specimens have an average density of 2.36 ± 0.04 g/cm^3.

1.4.3 Brazilian tension test

The Brazilian tension test performed under uniaxial stress state and biaxial stress state on varied bedding planes from 0 to 90 degrees. Both stress states depend on the stress distribution of Brazilian tension test by the formula of Hondros (1959). The y-axial stress is increased until failure occurs. Two strain gages are installed mutually perpendicular on two faces at the center of specimens to measure the lateral and axial deformations. The load at failure modes is recorded. They are used to calculate the strength and elastic parameters of the specimens.

1.4.4 Uniaxial stress state

Strain gages are installed with angles (θ) equal 60° (to measure ε_r) and 150° (to measure ε_θ) from x-axis. To obtain compressive elastic parameter of Phu Phan sandstone with bedding planes normal and parallel to the core axis.

1.4.5 Biaxial stress state

Strain gages are installed making angle (θ) equal to 0° (parallel to loading direction), and 90° (normal to loading direction) from x-axis. To obtain tensile strength and tensile elastic parameter of Phu Phan sandstone with bedding planes normal and parallel to the core axis.

1.4.6 Analysis of test results

The results obtained from Brazilian tension test under uniaxial stress state and biaxial stress state are compared to other researchers and analyzed to determine the mathematical relationship equations for use to predict the strength and elastic parameters of the Phu Phan sandstone.

1.4.7 Numerical simulations

Finite element analysis with different bedding plane orientations is performed by Phase2. Based on simulations of Brazilian tension test, to determine horizontal stress distribution and horizontal displacement on disk boundary. The analysis is in plane stress conditions. The results can reveal the effect of transverse

isotropy on the deformation behavior of sandstone under varying bedding plane orientations from 0° to 90° with 15 intervals.

1.4.8 Discussions, conclusions and thesis writing

Discussions are made on the reliability and adequacies of the approaches used here. Future research needs are identified. All research activities, methods, and results are documented and compiled in the thesis. The research or findings are published in the conference proceedings and journal.

1.5 Thesis content

This research thesis is divided into eight chapters. Chapter I introduces the thesis by briefly describing the background and rationale, research objectives, scope and limitations, and research methodology. Chapter II presents the summary results of the literature review about the effect of transversely isotropic on tensile strength, the effect of transversely isotropic on elastic parameters, degree of anisotropy, and numerical simulations under Brazilian tension test. Chapter III describes sample preparation. Laboratory testing is described in Chapter IV. Testing results and failure mode are described in Chapter V. Chapter VI presents the analysis of test results. Chapter VII describes stress distributions and deformability using the numerical model method by Phase2. Chapter VIII presents the discussion, conclusions, and recommendations for future studies.

CHAPTER II
LITERATURE REVIEW

2.1 Introduction

This chapter summarizes the results of literature review to improve an understanding of transverse isotropic rocks under tension. The stress distributions, the tensile strength, and elastic parameters of transverse isotropic rocks, and numerical simulations under Brazilian tension test are described. It is helpful to analyze and discuss the experimental results in this study.

2.2 Effect of transverse isotropic on tensile strength

Liao et al. (1997) study the direct tensile behavior of transversely isotropic rock on argillite based on ASTM D2936-08. The results indicate that tensile strength increases when the bedding plane approaching the loading direction. The curve of stress-strain at a high inclination angle ($\theta \geq 45°$), is quasi-liner, and exhibits a convex-upward before specimen failure. In contrast to the low inclination angle ($\theta \leq 45°$), the curve is non-linear and presents a concave-upward trend before specimen failure, as shown in Figure 2.1. They can be classified into modes of failure are two types, including a saw-toothed type with an inclination angle closer to 90° perpendicular to bedding plane, and a low inclination angle with a smooth type along foliation. It depends on bedding planes are normal or parallel to loading direction.

Chen and Hsu (2001) study the tensile strength of transverse isotropy rocks on marble from Hualien (Taiwan) by ring test and Brazilian tension test. The results indicate that tensile strength decrease with increasing bedding plane orientations under both ring test and Brazilian tension test. In addition, the boundary element method (BEM) analysis indicates that the maximum stress is present at the center point while the ring tests can avoid the bi-axial stress state that occurs in Brazilian tension test. This is a reason why the tensile strength of ring test is higher than Brazilian tension test, as shown in Figure 2.2. In order to represent a simple method and more in-situ conditions without the direct tension test, the Brazilian tension test is a significantly interesting approach.
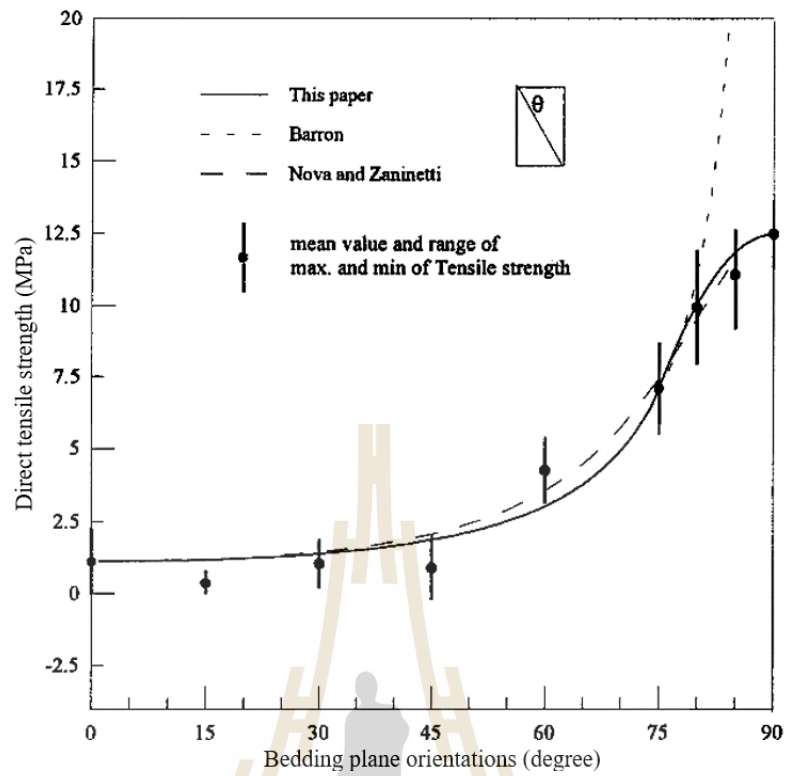
Figure 2.1 Direct tensile strength as a function of bedding plane orientations
(Liao et al., 1997).
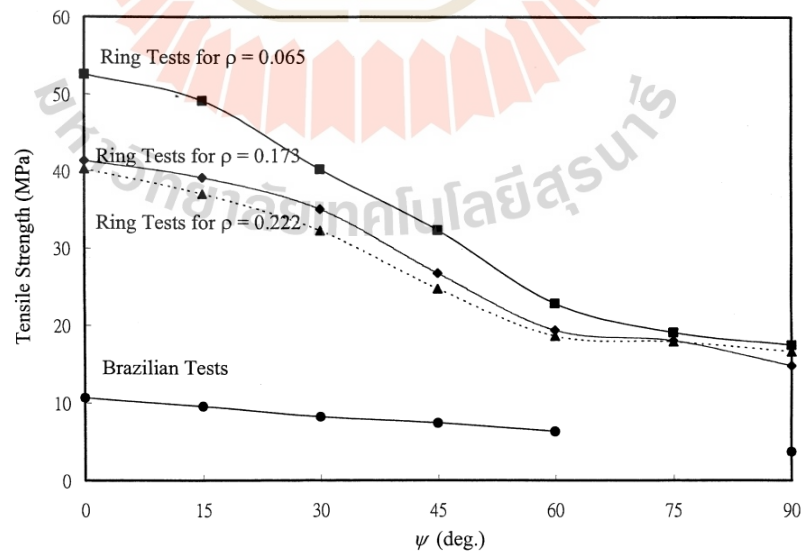
Figure 2.2 Tensile strength as function of bedding plane orientations under ring test
and Brazilian tension test (Chen and Hsu, 2001).

Hondors (1959) perform Brazilian tension test to determine strength, Young's modulus, and Poisson's ratio for concrete. Under diameter loading, the compressive stress at the center of disk is three times of the tensile stress. This method assumes that the Young's modulus and Poisson's ratio under compression and tension are the same for most rocks. The Young's modulus (E) and Poisson's ratio (v) can be calculated by

$$E = 2P(1-v^2)/(\pi Dt(\varepsilon_x + v\varepsilon_y)) \tag{2.1}$$

$$v = -(3\varepsilon_x + \varepsilon_y)/(3\varepsilon_y + \varepsilon_x) \tag{2.2}$$

where P is applied load, D is specimen diameter, t is thickness diameter, ε_x, ε_y is the strain along and normal to the load diameter at the center of the cylinder.

Ma and Hung (2008) present exact full-field solutions of stress, strain, and displacement of a circular disk to propose stress field inside under partially diametral distributed compressions. These solutions are combined with the Kirsch's solution with the known stress state of the solid disk. The Ma and Hung's formulation can be used to calculate stress in any point of disk using equations (2.3) and (2.4), as follows:

$$\sigma_r = \frac{P(1-\rho^2)(\rho^4+2\rho^2-1+2\cos2\theta)}{\pi Rt(\rho^4+1+2\rho^2 2\cos2\theta)^2} \tag{2.3}$$

$$\sigma_\theta = \frac{P(\rho^8+4\rho^4-4\rho^2-1-2(-2\rho^6+\rho^4+1)}{\pi Rt(\rho^4+1+2\rho^2 2\cos2\theta)^2} \tag{2.4}$$

where P is the total applied load, t is the thickness of disk, ρ is r/R, r is the radial distance, R is disk radius, and θ is the angle between x-axis and radial stress (σ_r) are shown in Figure 2.3.
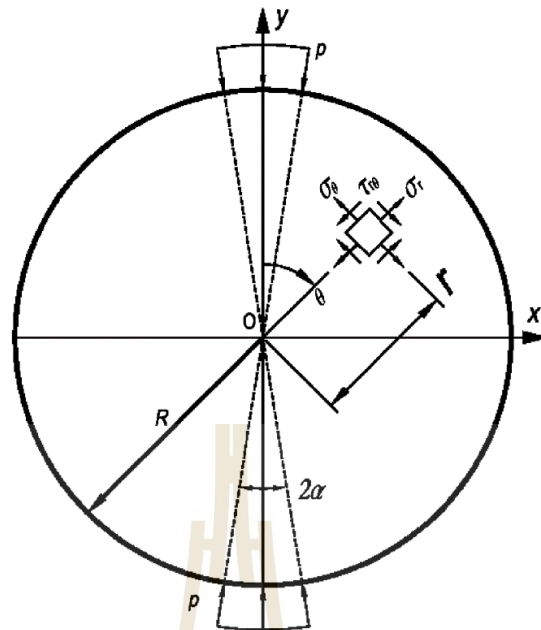
Figure 2.3 Disk of Brazilian tension test on radial and tangential stress
(Ma and Hung, 2008).

Chen et al. (1998) study the tensile strength and deformability of anisotropic rock on four types bedded sandstone to determine elastic constants by Brazilian tests and uniaxial compression tests. The tests method is conducted with the inclination angles (ψ) of 0°, 15°,30°,45°, 60°, 75° and 90° which all specimens assumed to be transverse isotropic. The results of elastic constants derived from Brazilian tests are compared with those obtained from uniaxial compression tests that are used to explain value of the stress concentration factor (q_{xx}) charts by complex variable function method and generalized reduced gradient method, as shown in Figure 2.4. The tensile strength can be calculated from stress concentration factor (q_{xx}) is given by:

$$\sigma_t = - q_{xx}(W_f)\pi Dt \tag{2.5}$$

where W_f is failure load when specimen fails, t is specimen thickness, D is specimen diameter, q_{xx} is the stress concentration factor. The stress concentration factor (q_{xx}) of -2 expected for isotropic case. On the other hand, the stress concentration factor (q_{xx}) of anisotropic rocks is more complex and depends on the elastic constants and the inclination angle (ψ). Thus, the complexity of determining the value on some convenient charts (Figure 2.5).
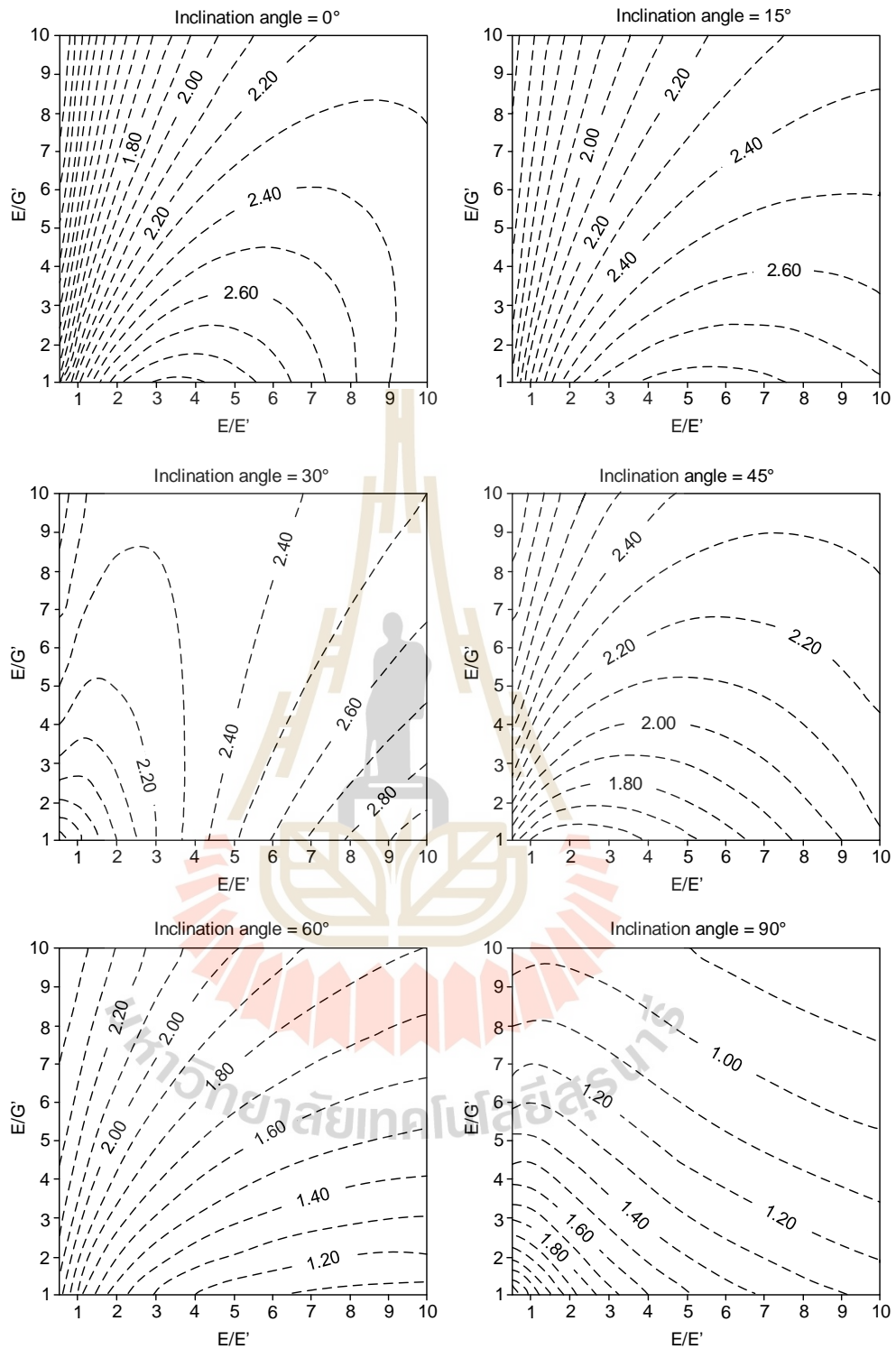
Figure 2.4 E/G' as a function of E/E' and each block vary of inclination angles for determine the stress concentration factor (q_{xx}) (Chen et al., 1998).
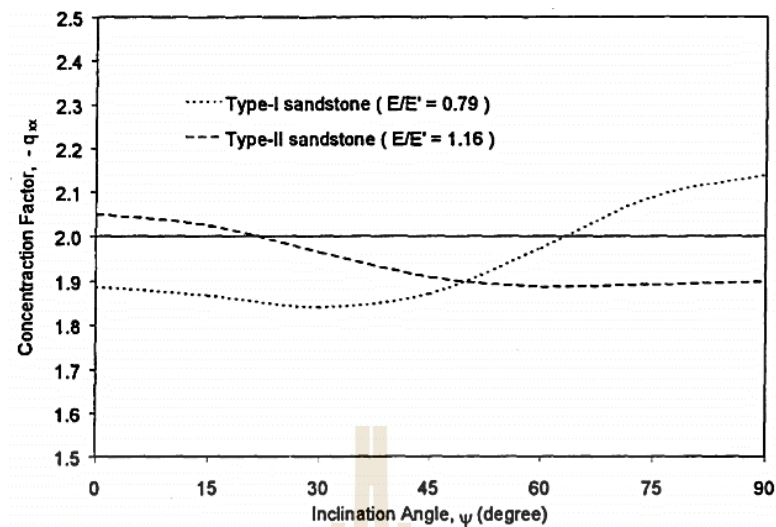
Figure 2.5 Concentration factor, -q_{xx} as a function of inclination angle, ψ (degree). The solid line of the isotropic case (Chen et al., 1998).

Tavallali and Vervoort (2010) study the tensile strength of Modave sandstone under different bedding plane orientations by Brazilian tension tests. The result shows that the tensile strength increases and then decreases with the bedding plane from 0° to 90°. According to the results, greater fracture length correlates with greater strength and applied energy. The variance in Brazilian tensile strength and applied energy as a function of total fracture length is more important than when considered as a function of inclination angle. It is the reason why for the specimens with different bedding planes but similar failure mode.

Khanlari et al. (2015) study the strength of laminated sandstones under uniaxial compressive strength, point load, and Brazilian tension tests. The results indicate that the correlation between uniaxial compressive strength and bedding planes show the asymmetrical shoulder-shaped curve which minimum strength at β =30°. The correlation between Brazilian strength and bedding planes as well as point load index and bedding planes shows the direct linear relationship that the maximum at 90° and the minimum at 0°. Figure 2.6 shows Brazilian strength with bedding plane orientations.

Zhang et al. (2016) study influence of transverse isotropy on tensile strength of bedded sandstone from three gorges reservoir region in Zigui under various bedding planes from 0° to 90°. The tensile strength gradually increases with increasing of bedding plane orientations, when $\theta \leq 15°$ and $\theta \geq 75°$ is slow increasing trend and noticeable when $15° \leq \theta \leq 75°$, as shown in Figure 2.7.
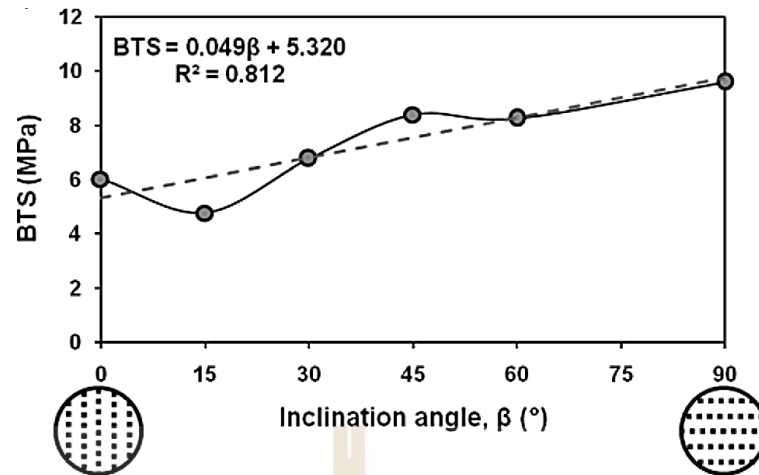
Figure 2.6 Relationship of Brazilian tension tests with bedding plane orientations (Khanlari et al., 2015).
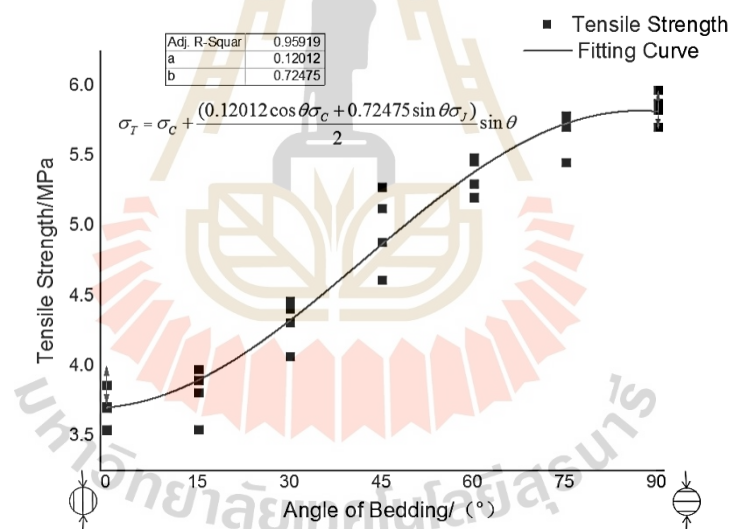
Figure 2.7 Tensile strength of sandstone under various bedding plane orientations (Zhang et al., 2016).

Han et al. (2020) conduct on the Brazilian splitting test on slate specimens from Muzhailing tunnel in Northwest China. with various inclination angle. The result of indirect tension is evaluated in terms of tensile strength, tensile failure behavior relative to the roughness of failure fracture, applied energy, and acoustic emission (AE) characteristics. Furthermore, the indirect tensile failure mechanism of slate with different inclination angles is also elucidated. The failure behavior on inclination angle

is less than 45° risen on the surface fracture in the middle of specimen. On the other hand, the surface fracture of inclination angle is larger than 45° risen on noncentral, especially for the sample with 90°. Hence, at the bedding angle when β = 0° and 90°, the tensile failure occurs along the bedding plane and at slate substrate. Consequently, when β = 30° to 60°, failure mode of the specimen was tensile and shear composite failure.

Yang et al. (2020) study the behavior of transverse isotropic shale from Lushan city in China by conventional triaxial tests and Brazilian tests. The damage and cracks of conventional triaxial tests is occur easily in bedding planes when low confining pressure and uniaxial compression. Cohesion of bedding angle = 90° less than that bedding angle = 0°. However, bedding angle = 90° are more sensitive to confining pressure leads to friction angle of bedding angle = 90° higher than that bedding angle = 0°. The result of Brazilian tension test is specimen group II is less Brazilian tensile strength than specimen group I which group II vary inclination angle. The Brazilian tensile strength of group II at inclination angle below 45° is lower than that exceed 45°. According to the results, state that the bedding planes have significant effect on tensile strength.

The Brazilian tensile strength usually depends on the failure modes under Brazilian tension test. Therefore, this study can be classified into five categories with Ma et al. (2018): (1) tensile failure across the bedding planes occurs once the bedding plane is perpendicular to the loading direction, (2) shear failure across the bedding planes occurs when the bedding plane has a low angle, (3) tensile failure along the bedding planes occurs once the bedding plane is parallel to the loading direction, (4) shear failure along the bedding planes occurs when the bedding plane has a highly angle, and (5) mixed failure.

2.3   Effect of transversely isotropy on elastic parameters

Amadei (1996) analyzes elastic modulus for transverse isotropic rock by using five parameters (E, E', v, v', G') with the following definitions:

- E and E' are young's moduli in the plane of transverse isotropic and in direction normal to it.

- v and v' are Poisson's ratios characterizing the lateral strain response in the plane of transverse isotropic to a stress acting parallel or normal to it, respectively.

- G' is the shear modulus in planes normal to the plane of transverse isotropic.

The mean strain components $(\varepsilon_x, \varepsilon_y, \varepsilon_{xy})$ is the mean displacement components $(a_{11}, a_{12}, ..., a_{66})$, and the mean stress components $(\sigma_x, \sigma_y, \sigma_{xy})$ in x-y plane, as follows:

$$\begin{Bmatrix} \varepsilon_x \\ \varepsilon_y \\ \gamma_{xy} \end{Bmatrix} = \begin{bmatrix} a_{11} & a_{12} & a_{16} \\ a_{12} & a_{22} & a_{26} \\ a_{16} & a_{26} & a_{66} \end{bmatrix} \times \begin{Bmatrix} \sigma_x \\ \sigma_y \\ \tau_{xy} \end{Bmatrix} \tag{2.6}$$

The x-y coordinate system can be calculating of a_{11}, a_{12}, ..., $a66$ from equations:

$$a_{11} = \frac{\sin^4 \psi}{E'} + \frac{\cos^4 \psi}{E} + \frac{\sin^4 2\psi}{4}\left(\frac{1}{G'} - \frac{2\nu'}{E'}\right) \tag{2.7}$$

$$a_{12} = \frac{\sin^4 2\psi}{4}\left(\frac{1}{E'} + \frac{1}{E} - \frac{1}{G'}\right) - \frac{\nu'}{E'}\left(\cos^4 \psi + \sin^4 \psi\right) \tag{2.8}$$

$$a_{16} = \sin 2\psi\left[\frac{\sin^2 \psi}{E'} + \frac{\cos^2 \psi}{E}\right] + \left(\frac{1}{2G'} - \frac{\nu'}{E'}\right)\cos 2\psi \tag{2.9}$$

$$a_{22} = \frac{\cos^4 \psi}{E'} + \frac{\sin^4 \psi}{E} + \frac{\sin^4 2\psi}{4}\left(\frac{1}{G'} - \frac{2\nu'}{E'}\right) \tag{2.10}$$

$$a_{26} = \sin 2\psi\left[\frac{\cos^2 \psi}{E'} + \frac{\sin^2 \psi}{E}\right] - \left(\frac{1}{2G'} - \frac{\nu'}{E'}\right)\cos 2\psi \tag{2.11}$$

$$a_{66} = \sin^2 2\psi\left(\frac{1}{E'} + \frac{1}{E} - \frac{2\nu'}{E'}\right) + \frac{\cos^2 2\psi}{G'} \tag{2.12}$$

According to the testing, the loading assumed angle is 2α, and P = W/(αDt) where W is the load applied on disc in the y direction, as shown in Figure 2.8. The components of the stress filed can be calculate by

$$\sigma_x = q_{xx}\frac{W}{\pi Dt}; \qquad \sigma_y = q_{yy}\frac{W}{\pi Dt}; \qquad \tau_{xy} = q_{xy}\frac{W}{\pi Dt} \tag{2.13}$$

where q_{xx}, q_{yy}, and q_{xy} is the stress concentration factors, W is diametral load at angular width 2α, D is the diameter of rock, t is the thickness of rock. The stress concentration factors (q_{xx}, q_{yy}, q_{xy}) dependent with dip angle (ψ) and ratios of elastic constants is E/E', E/G' and v'. when substitute equation (2.13) into equation (2.6), equation becomes

$$\frac{\pi Dt}{W}\begin{Bmatrix}\varepsilon_x \\ \varepsilon_y \\ \gamma_{xy}\end{Bmatrix} = \begin{bmatrix} a_{11} & a_{12} & a_{16} \\ a_{12} & a_{22} & a_{26} \\ a_{16} & a_{26} & a_{66} \end{bmatrix} \times \begin{Bmatrix} q_x \\ q_y \\ q_{xy} \end{Bmatrix} \tag{2.14}$$

The elastic of transverse isotropic obtain from two specimen group, the plane is parallel of transverse isotropic as shown in Figure 2.8(a) to determine E and v of isotropic, which this condition use value q_{xx} = -2, q_{yy} = 6 and q_{xy} = 0 on equation 2.15. the plane is perpendicular of transverse isotropic as shown in Figure 2.8(b) to determine E', v' and G', which depend on orientation from equation 2.16.

$$\frac{\pi Dt}{W}\begin{Bmatrix}\varepsilon_x \\ \varepsilon_y \\ \gamma_{xy}\end{Bmatrix} = \begin{bmatrix} 1/E & -v/E & 0 \\ a_{12} & 1/E & 0 \\ 0 & 0 & 2(1+v)/E \end{bmatrix} \times \begin{Bmatrix} -2 \\ 6 \\ 0 \end{Bmatrix} \tag{2.15}$$

$$\frac{\pi Dt}{W}\begin{Bmatrix}\varepsilon_x \\ \varepsilon_y \\ \gamma_{xy}\end{Bmatrix} - \frac{1}{E}\begin{Bmatrix}C_x \\ C_y \\ C_{xy}\end{Bmatrix} = \begin{bmatrix} T_{11} & T_{12} & T_{13} \\ T_{21} & T_{22} & T_{23} \\ T_{31} & T_{32} & T_{33} \end{bmatrix} \times \begin{Bmatrix} 1/E' \\ -v/E' \\ 1/G' \end{Bmatrix} \tag{2.16}$$

where C_1, C_2, C_3, T_{11}, ..., T_{33} are dependent of inclination angle and q_{xx}, q_{yy}, and q_{xy}. The elastic constants of transverse isotropic select from thermodynamic constraints, that must be satisfied

$$E, E', G, \text{and } G' > 0 \qquad 1 - v - 2\frac{E}{E'}(v')^2 > 0 \tag{2.17}$$

Three unknowns are 1/E', v'/E and 1/G' of equation (2.12) constrained by the inequalities in equation (2.17).
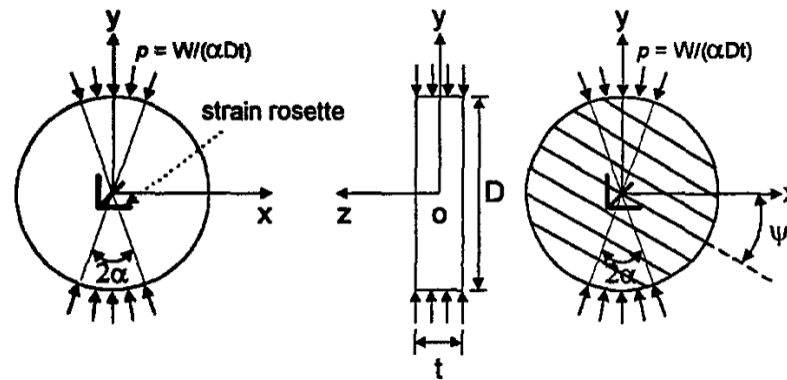
Figure 2.8 Diametral compression of a thin disc over an angular width of 2α.
(a) Loading in the plane of transversely isotropy, (b) loading in the
plane perpendicular to the plane of transversely isotropy
(Chen et al., 1998).

Liao et al. (1997) study transverse isotropic rock in direct tension test to
determine the five elastic constants. The E and v perform on specimen with bedding
planes parallel to tensile direction. On the other hand, the E', v' and G' results
obtained from testing on specimen with an inclination angle of foliation planes
perpendicular to tensile direction. The results show the elastic moduli of transverse
isotropic rock obtained from the uniaxial tensile test are more conservative when
compare with uniaxial compression test, as shown in Table 2.1.

Chen et al. (1998) study deformability of transverse isotropic on sandstone.
The prepare of specimen with layers dipping at different bedding planes between
0° to 90°. The testing can be determining the three elastic constants including E', v'
and G'. The test results show the average values of elastic constants as E' = 3.6×106 psi,
v' = 0.128 and G' = 1.8×106 psi, as shown in Figure 2.9.

Table 2.1 Elastic constants of argillite specimen under tension and compression
(Liao et al., 1997).

Specimen, dip angle (q)	E (GPa)	v	E' (GPa)	G' (GPa)	v' (GPa)	Test compression
30			51.14	15.61	0.22	Direct
45	59.09	0.22	51.86	14.91	0.10	tension
20			37.28	12.36	0.16	Uniaxial
45	51.82	0.19	32.24	13.26	0.18	compression
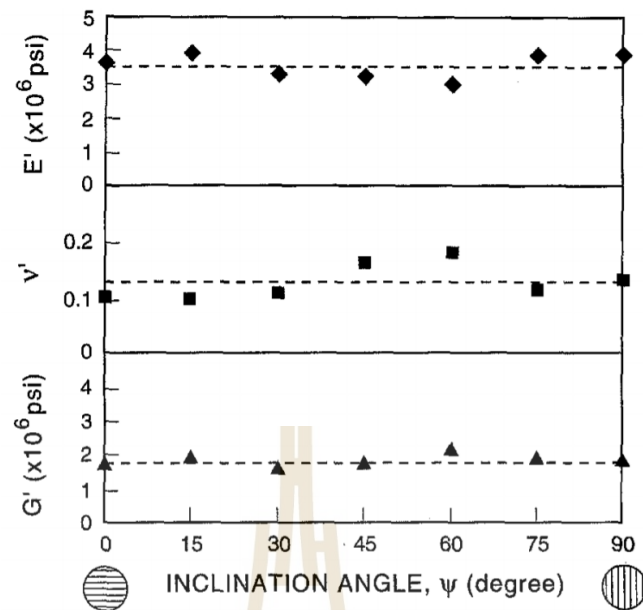
Figure 2.9 E', ν' and G' as a function of the inclination angle, ψ (Chen et al., 1998).

Jianhong et al. (2009) state that elastic modulus of compression (Ec) is different from elastic modulus of tensile (Et) of rock, due to microcracks and inhomogeneity. The tensile elastic modulus (Et) obtains from direct tension tests. However, the direct tension test of rock is difficult to prepare specimens and perform, forasmuch as stress concentrations. The developed a new method to determine Et of rock is two strain gauges to record tensile strain are installed at center of a Brazilian disc's two side faces in the direction perpendicular to the loading diameters, and a force sensor is used to record the force applied. The tensile elastic modulus can be calculated from formulas on the basis of elasticity theory. The test results for limestone, sandstone, granite, and marble show that tensile elastic modulus is less than compressive elastic modulus, and the ratio is between 0.6 to 0.9.

Fuenkajorn and Klanphumeesri (2010) propose compression to tension load converter (CTC) which is a new loading device used for unidirectional tensile stress to prepare specimen on dog-bone shaped. The device also allows a measurement of rock Poisson's ratio and elastic modulus under compressive stresses and uniaxial tensile. Efficiency is assessed to determining direct tensile strength and stiffness of intact specimens prepared form Saraburi limestone, Saraburi marble and Phu Phan sandstone at laboratory. For all tested rocks on direct tensile strengths are less than ring and Brazilian tensile strengths in Table 2.2. The value of Poisson's ratios and elastic moduli under uniaxial tension are less than those under uniaxial compression in

Table 2.3. The dislocation relates to amount and distribution of micro-fissures and pore spaces, and bond strength of cementing materials. It is assumed that effort required to dilate pore spaces on tensile loading is less than that to withdraw them on compressive loading.

Table 2.2 Summary of direct and indirect tensile strengths.

Rock Type	Density (g/cc)	Direct tensile strength (MPa)	Brazilian tensile strength (MPa)	Ring tensile strength (MPa)
PP sandstone	2.36 ± 0.12	6.49 ± 0.22	10.68 ± 0.70	16.10 ± 3.00
SB marble	2.65 ± 0.08	6.33 ± 0.62	8.02 ± 0.25	20.59 ± 1.24
SB limestone	2.81 ± 0.05	9.31 ± 0.65	10.90 ± 0.19	23.18 ± 1.70

Table 2.3 Elastic parameters from compressive and tensile loadings.

Rock Type	Elastic modulus (GPa)		Poisson's Ratio	
	E_c	E_t	v_c	v_t
PP sandstone	16.23 ± 1.95	6.73 ± 0.35	0.17 ± 0.011	0.05 ± 0.005
SB marble	41.66 ± 2.08	34.43 ± 0.95	0.19 ± 0.010	0.15 ± 0.003
SB limestone	37.15 ± 0.99	26.13 ± 1.06	0.21 ± 0.012	0.18 ± 0.005

2.4 Degree of anisotropy

The anisotropy of intact rock can be characterized by the degree of anisotropic (R_c) which are determined by Ramamurthy (1993), Hakala et al. (2007), Ismael et al. (2014), and You et al. (2021) as:

$$R_c = \sigma_{max} / \sigma_{min} \tag{2.18}$$

where σ_{max} is uniaxial compressive strength normal to the bedding and σ_{min} is minimum uniaxial compressive strength. The classification given in Table 2.4.

Ma et al. (2018) reviews the state of the art in the experimental studies on Brazilian tensile strength of anisotropic rocks to predict the tensile strength. The results state that this method can be used to predict the tensile strength and failure mode of anisotropic rocks. Degrees of anisotropy are obtained by Brazilian tensile strength on

equation (2.11). Table 2.5 show the statistical results of degree of anisotropic for various bedding plane orientations. Abbass et al. (2019) review method and accumulate the equation of anisotropy degree are shown in Table 2.6.

Table 2.4 Degrees of anisotropic and rock classes (Ramamurthy et al., 1993).

R_c	Rock class
$1.0 < R_c < 1.1$	Isotropic
$1.1 < R_c < 2.0$	Low anisotropic
$2.0 < R_c < 4.0$	Medium anisotropic
$4.0 < R_c < 6.0$	High anisotropic
$6.0 < R_c$	Very high anisotropic

Table 2.5 Statistical results of degree of anisotropic under tensile strength (Ma et al., 2018).

Rock Types	Value	Degrees of anisotropy
Shale	1.30-5.01	Weak - Strong
Sandstone	1.14-4.50	Weak - Strong
Slate	1.82-4.10	Weak - Strong
Gneiss	1.39-3.06	Weak - Medium
Schist	2.75-6.63	Medium - Strong
Coal	1.18-1.80	Weak
Marl	1.61-1.82	Weak

Table 2.6 Formula of degree of anisotropic (Abbass et al., 2019).

No.	Formula	Resources
1	$K_1 = (\sigma_1 - \sigma_3)\| / (\sigma_1 - \sigma_3)\perp$ $K_2 = (\sigma_1 - \sigma_3)_{max} / (\sigma_1 - \sigma_3)_{min}$	Niandou et al. (1997)
2	$R_c = \sigma_{c,max} / \sigma_{c,min}$	Duveau and Shao (1998)
3	$R_c = \sigma_{c,90°} / \sigma_{c,60°}$	Tien et al. (2006)
4	$f = \sigma_{1,max} - \sigma_{1,min} / \sigma_{1,max}$	Wu et al. (2016)
5	$SA1 = \sigma_{1,max} / \sigma_{1,min}$ $SA2 = \sigma_{1,max} - \sigma_{1,min}$	Cheng et al. (2017)

Note: K_1, K_2, R_C, f, SA1, and, SA2 is degree of anisotropy.

2.5   Numerical simulations under Brazilian tension test

Dan (2011) simulates the Brazilian tension test on transverse isotropic rocks under FLAC3D. The code is based on the explicit finite-difference method with 81 grid points in the tetrahedral mesh. The extreme mesh resolution in order to duly show the complicated failure patterns and locally large stress gradients. The load is applied by two lading jaws. The simulation shows the stress distribution and failure state in Figure 2.9. The comparison result of tensile strength states that the numerical values are close to laboratory results, while the numerical model can be used to observe the failure pattern.

Tan et al. (2015) study the tensile strength and failure zone of Brazilian disc for anisotropic rocks under UDEC simulation. Numerical simulation using discrete element modeling. The slate specimen is represented by deformable blocks, which are cemented to each other along with their contacts. The bedding planes (weak planes) are represented by joints with lower strength. The parallel joints have a spacing of 0.3 mm. The results indicate that the tensile strength obtained by laboratory results shows a similar tend to numerical simulations, while the fracture pattens observers in laboratory are similar with tensile stress distribution contour and fracture opening by numerical simulations, as shown in Figure 2.10.

Li and Wong (2013) study crack initiation of Brazilian disk using a linear elastic model by $FLAC^{3D}$ on strain and stress distributions. They found that the crack initiation point was approximately 5 mm (the radius is 25 mm) away from the two loading points, and found that the crack initiation point occurred 0.8 R (R is the radius) away from the center of disk by Markides and Kourkoulis (2012). On other hand, the failure of the Brazilian disc begins as an extension fracture in the center (interior) of the disk and then propagates to the top and bottom surfaces by Van De Steen et al. (2005) on the boundary element code DIGS (Discontinuity Interaction and Growth Simulation), Zhu and Tang (2006) using numerical simulator based on RFPA (Rock Failure Process Analysis), and Cai and Kaiser (2004) using FEM to the fracture criterion within the intact rock and then represented the crack is initiated by DEM.
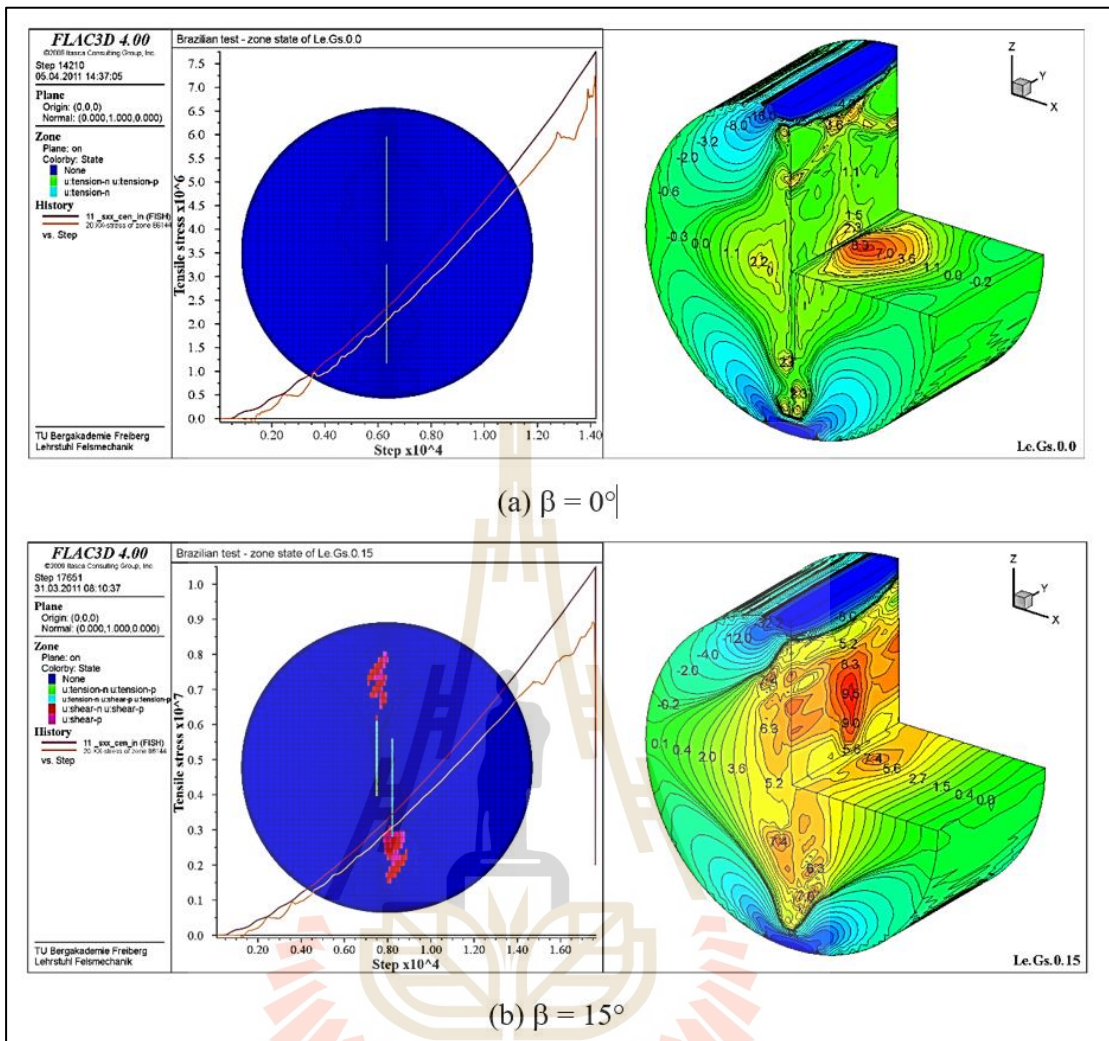
Figure 2.10 Tensile stress distribution contour and failure state under different bedding planes by FLAC^{3D}: (a) $\beta = 0°$ and (b) $\beta = 15$ (Dan, 2011).

(a) β = 30°

(b) β = 45°
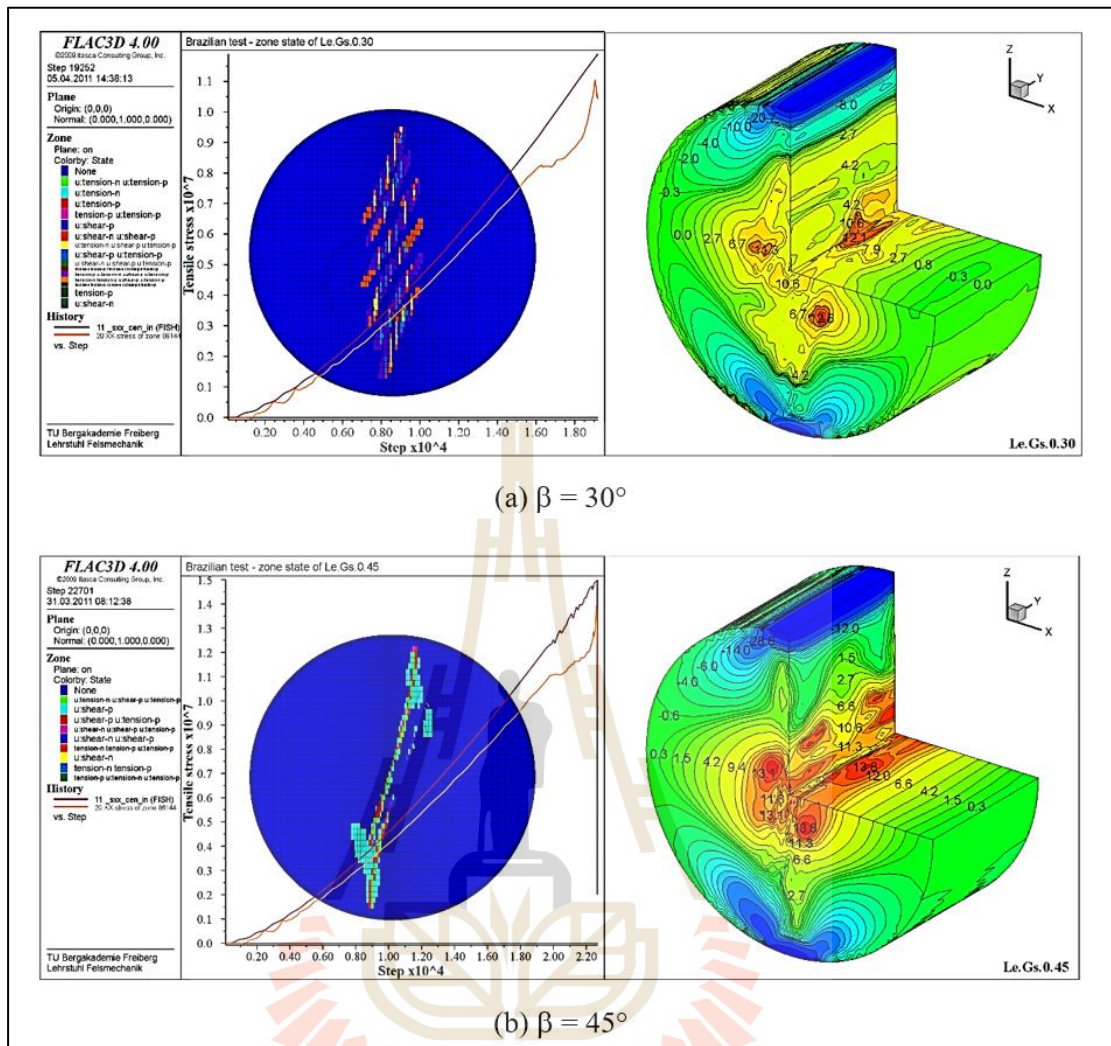
Figure 2.11 Tensile stress distribution contour and failure state under different bedding planes by FLAC[3D]: (a) β = 30° and (b) β = 45° (Dan, 2011).
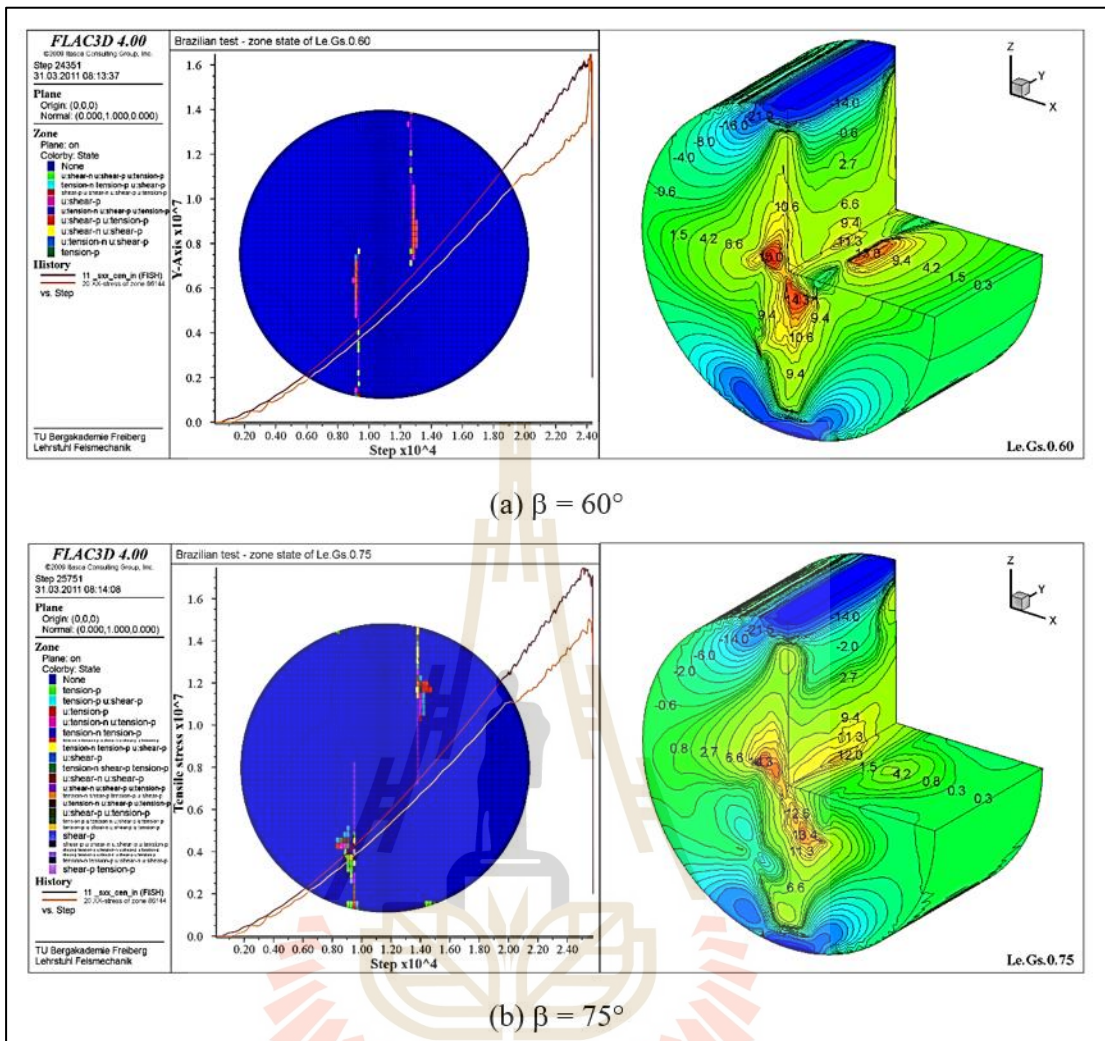
Figure 2.12 Tensile stress distribution contour and failure state under different bedding planes by FLAC^{3D}: (a) β = 60° and (b) β = 75° (Dan, 2011).

β = 90°

Figure 2.13 Tensile stress distribution contour and failure state under different bedding planes by FLAC^{3D} for β = 90° (Dan, 2011).
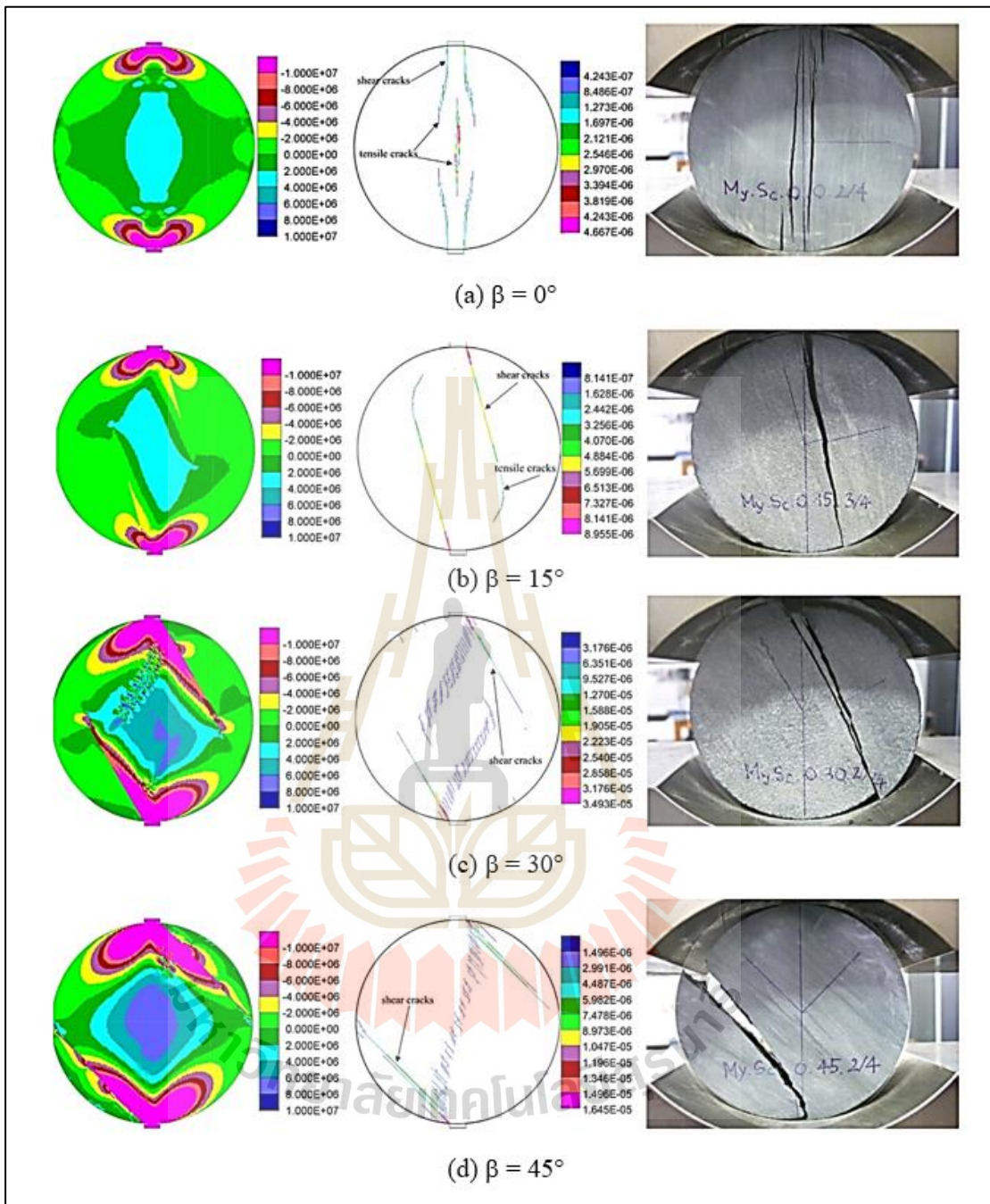
Figure 2.14 Tensile stress distribution contour and fracture opening under different bedding planes by UDEC for β = 0°, 15°, 30° and 45° (Tan et al., 2018).
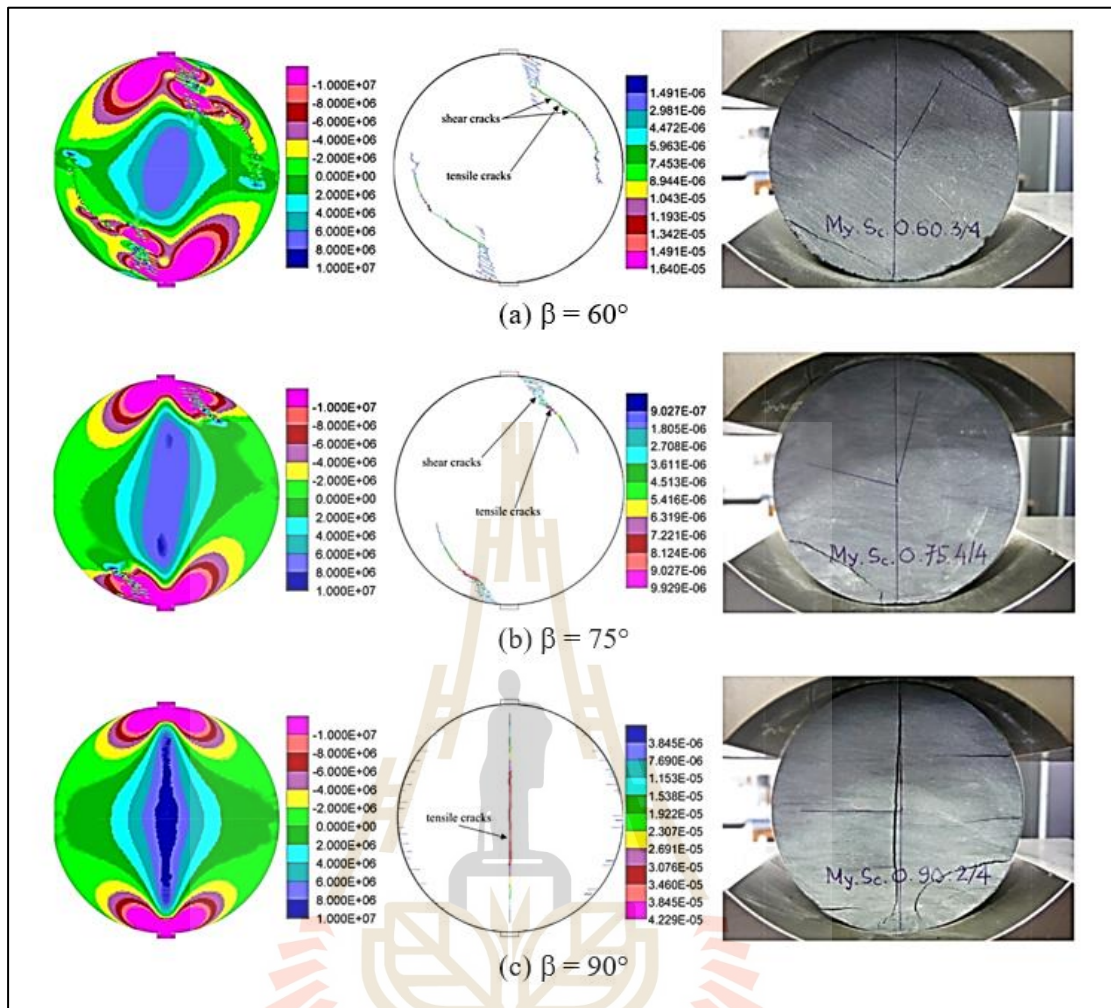
Figure 2.15 Tensile stress distribution contour and fracture opening under different bedding planes by UDEC for β = 60°, 75° and 90° (Tan et al., 2018).

CHAPTER III
SAMPLE PREPARATION

3.1 Introduction

This chapter describes the sandstone sample preparation to be used in the Brazilian tension testing. The specimen dimensions are given. The rock is obtained from Phu Phan formation.

3.2 Sample preparation

Several sandstone blocks are collected from a quarry in Saraburi province. The selection criteria for this sandstone are the availability and well-defined bedding planes. The sandstone blocks are cored to obtain nominal diameters of 74 mm. The specimens are cut to obtain discs with nominal thickness (t) of 37 mm. The bedding planes are parallel (Fig. 3.1(a)) and normal (Fig. 3.2(b)) to the core axis, for use under two stress conditions: uniaxial and biaxial stress states. Eight specimens are prepared for each stress condition. Tables 3.1 and 3.2 show dimensions and density of the tested specimens.

3.3 X-ray diffraction analysis

The X-ray diffraction analysis is performed after the mechanical testing. The rock is ground to obtain power with particle sizes of less than 0.25 mm (mesh #60). The powder specimen is used to determine mineral compositions by X-ray diffraction (XRD) analysis. X-ray diffractormeter-D2 phaser is used. Table 3.3 gives the results.
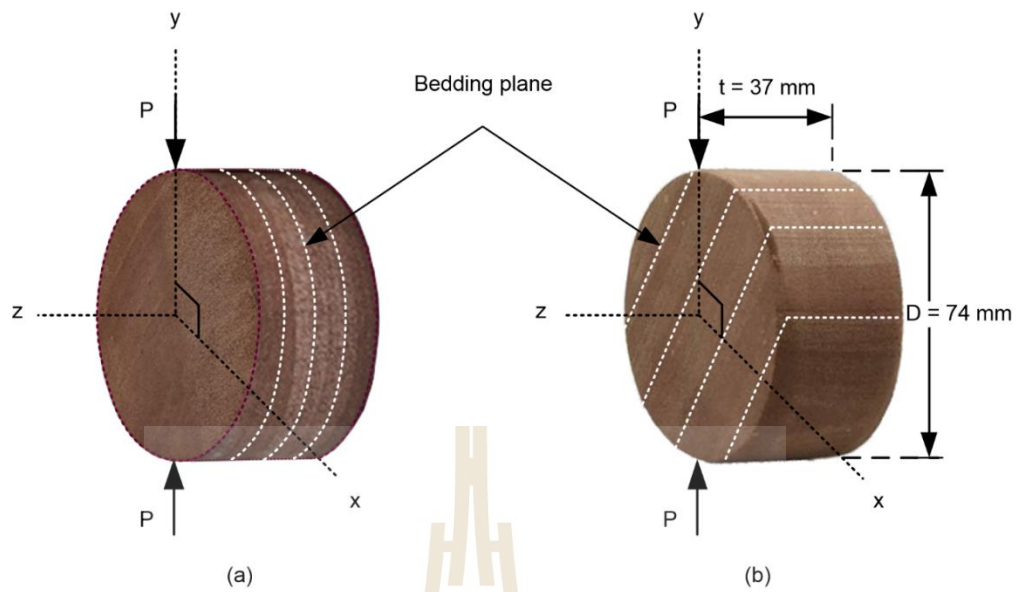
Figure 3.1 Examples of Phu Phan specimens: (a) bedding planes normal to core axis
(z-axis), and (b) bedding planes parallel to core axis.

Table 3.1 Phu Phan specimens prepared for Brazilian tension test to measure strain under
uniaxial stress direction.

Specimen Number	Average Diameter (mm)	Average Thickness (mm)	Weight (g)	Density (g/cc)
PP-BZ-Uni-01	73.90	39.00	394.31	2.36
PP-BZ-Uni-02	73.74	37.08	373.17	2.36
PP-BZ-Uni-03	73.76	36.04	359.70	2.34
PP-BZ-Uni-04	73.74	38.38	380.65	2.32
PP-BZ-Uni-05	73.72	37.64	378.58	2.36
PP-BZ-Uni-06	73.70	37.92	386.75	2.39
PP-BZ-Uni-07	73.80	39.67	399.67	2.36
PP-BZ-Uni-08	73.80	37.36	376.79	2.36
Mean ± SD				2.36±0.02

Table 3.2 Phu Phan specimens prepared for Brazilian tension test under biaxial stress.

Specimen Number	Average Diameter (mm)	Average Thickness (mm)	Weight (g)	Density (g/cc)
PP-BZ-Bi-01	73.94	37.46	378.6	2.35
PP-BZ-Bi-02	73.92	40.58	418.81	2.40
PP-BZ-Bi-03	73.88	40.54	415.91	2.39
PP-BZ-Bi-04	73.90	40.30	411.58	2.38
PP-BZ-Bi-05	73.72	39.80	405.41	2.39
PP-BZ-Bi-06	73.84	40.26	416.18	2.41
PP-BZ-Bi-07	73.90	42.00	428.43	2.38
PP-BZ-Bi-08	73.88	41.10	420.40	2.39
Mean ± SD				2.39±0.02

Table 3.3 Mineral compositions of Phu Phan specimen.

Mineral compositions (%by weight)											
Quartz	Kaolinite	Muscovite	Albite	Anorthite	Microcline	Calcite	Oligoclase	Chlorite	Illite	Andesite	Hematite
45.18	1.47	4.99	13.55	4.24	1.45	0.57	11.42	6.54	8.10	0.24	2.25

CHAPTER IV
LABORATORY TESTING

4.1 Introduction

The objective of this section is to describe the test method to determine Brazilian tensile strength and elastic parameters of the sandstone as affected by transverse isotropic texture (bedding planes). Two stress conditions are imposed: under uniaxial stress direction and biaxial stress. The tests are performed on specimens with bedding planes normal and parallel to the core axis. Calculation and test method follow ASTM D3967-16 standard. Figures 4.1 gives laboratory test arrangement and components used during the test.
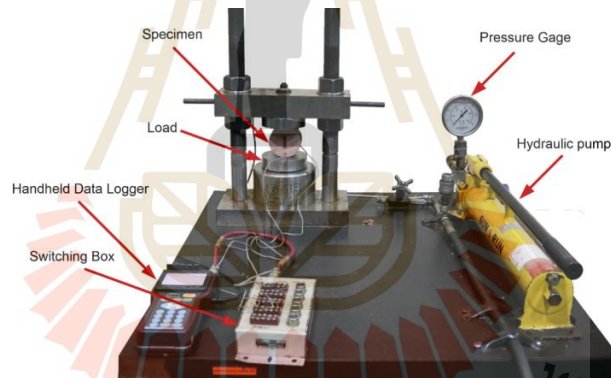
Figure 4.1 Brazilian tension test apparatus.

4.2 Measurement under uniaxial stress direction

Figure 4.2 shows the stress distribution of Brazilian tension test under plane stress condition (σ_x, $\sigma_y \neq 0$, and $\sigma_z = 0$). The analytical solution of the plane stresses gives the radial (σ_r) and tangential (σ_θ) stresses with mutually perpendicular directions.

The stress distribution can be used to design the direction of the installed strain gages for Brazilian tension test (under uniaxial stress direction and biaxial stress). A pair of strain gages (TML, PFL-20-11-1L, 10 mm) are installed to measure deformations at the center of the specimen in mutually perpendicular directions. The σ_r and σ_θ at the

center (crack initiation point) of the specimen with any angle (θ) can be calculated as (Ma and Hung, 2008):

$$\sigma_r = \frac{P(1-\rho^2)(\rho^4 + 2\rho^2 - 1 + 2\cos2\theta)}{\pi Rt(\rho^4 + 1 + 2\rho^2 2\cos2\theta)^2} \tag{4.1}$$

$$\sigma_\theta = \frac{P(\rho^8 + 4\rho^4 - 4\rho^2 - 1 - 2(-2\rho^6 + \rho^4 + 1)}{\pi Rt(\rho^4 + 1 + 2\rho^2 2\cos2\theta)^2} \tag{4.2}$$

where t is the thickness of disk, P is the total applied load, ρ is r/R, r is the radial distance, R is disk radius, and θ is the angle between x-axis and radial stress (σ_r).

4.3   Uniaxial stress direction

Strain gages are installed with angles (θ) equal 60° (to measure ε_r) and 150° (to measure ε_θ) from x-axis. At this angle, σ_r is twice of the Brazilian tensile stress, and σ_θ is equal to zero. This is primarily to obtain the compressive elastic modulus and Poisson's ratio. They can be determined for the specimens with bedding planes normal and parallel to the core axis. The compressive elastic modulus (E_{CP}) and Poisson's ratio (ν_θ) of specimens can then be obtained at any angle of the bedding planes when they are parallel to the core axis. When the beds are set normal to the core axis the elastic modulus and Poisson's ratio on the beds can be obtained. For the first case, the angle β varies from 0 to 90 degrees with 15 degrees interval.
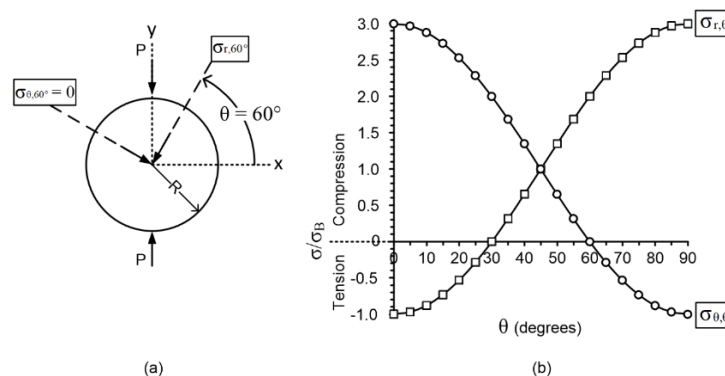
Figure 4.2 Radial and tangential stresses at disk center (Ma and Hung, 2008).
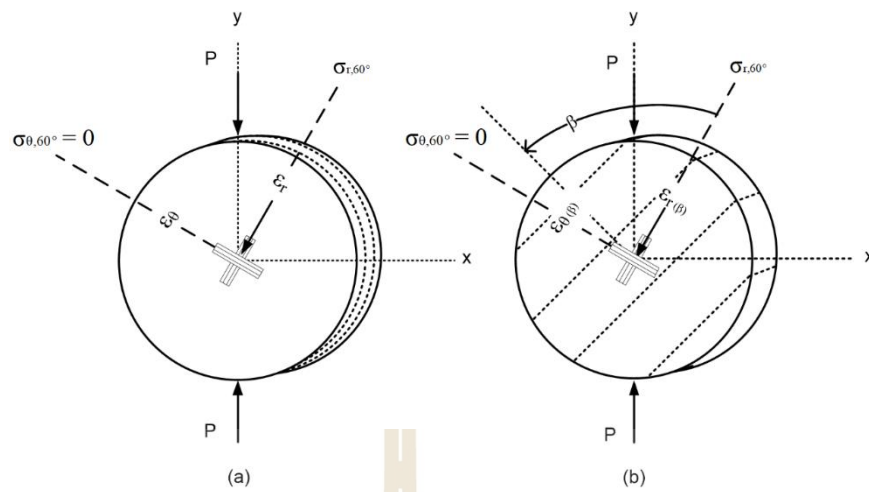
Figure 4.3 Specimens with strain gages installed under uniaxial stress direction:
(a) beds normal to sample axis, (b) beds parallel to sample axis with
strain gages making 60° and 150° with x-axis.

4.4 Test under biaxial stress state

Testing under biaxial stress state is obtained from a combination of compressive and tensile stresses resulting from the induced vertical and horizontal stresses at the specimen center. Strain gages are installed making angle (θ) equal to 0° (parallel to loading direction), and 90° (normal to loading direction). Under this condition, σ_r represents the Brazilian tensile stress, σ_θ is in compression with the magnitudes of three times the Brazilian tensile stress. The tensile elastic modulus (E_{TP}) of specimen with beds parallel to loading axis is shown in Figure 4.4(a). The tensile elastic modulus ($E_{TN(\beta)}$) of specimen with beds normal to loading axis where the angle β is the angle between loading direction and the normal of bedding planes as shown in Figure 4.4(b). The tensile modulus can be calculated from the measured compressive and tensile strains. They can be determined based on Hooke's law, as follows:

$$\varepsilon_x = \frac{\sigma_x}{E_{T(90°-\beta)}} - V_{T(\beta)}\frac{\sigma_y}{E_{C(\beta)}} \tag{4.3}$$

$$\varepsilon_y = \frac{\sigma_y}{E_{C(\beta)}} - V_{T(\beta)}\frac{\sigma_x}{E_{T(90°-\beta)}} \tag{4.4}$$

where ε_x is strain in x-direction, ε_y is strain in y-direction, σ_x is stress in x-direction, σ_y is stress in y-direction, $E_{T(\beta)}$ is tensile elastic modulus and $E_{C(\beta)}$ is compressive elastic modulus, obtained from the uniaxial test condition. The angle β is between the loading direction and the normal of bedding planes.
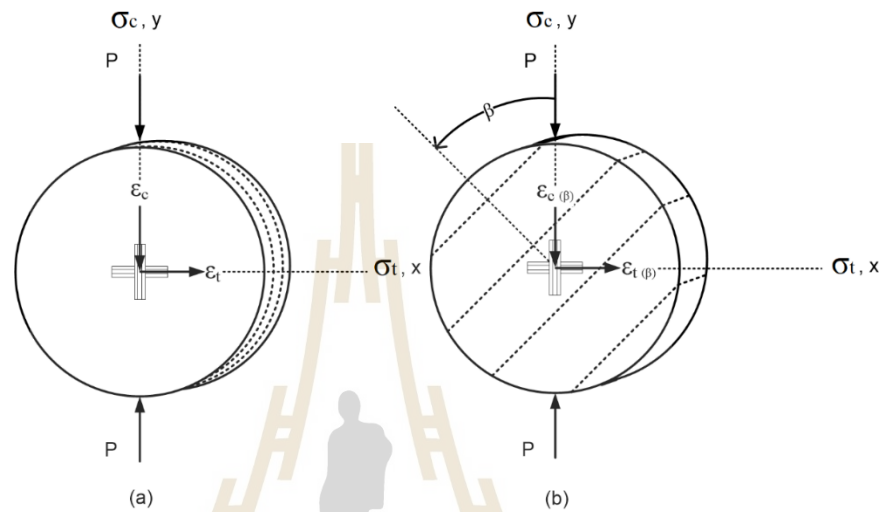
Figure 4.4 Specimens with strain gages installed under biaxial stress: (a) beds normal to sample axis, (b) beds parallel to sample axis with strain gages parallel and normal to loading direction.

CHAPTER V
TEST RESULTS

5.1   Introduction

This chapter describes the results obtained from Brazilian tension testing under uniaxial stress direction and biaxial stress state. They are presented in the forms of stress-strain curves, tensile strength, and deformation moduli. These parameters have been measured every 15 degrees from 0 to 90 degrees.

5.2   Test results of uniaxial stress direction

Figures 5.1 and 5.2 show the compressive stress-strain curves from start loading to failure under uniaxial test condition on specimens with bedding planes normal and parallel to the core axis. The stress-strain curves tend to show nonlinear behavior near the failure stress. The uniaxial stress is presented in the forms of loci of radial strains ($\varepsilon_{r,60°}$) and tangential strains ($\varepsilon_{\theta,150°}$) as a function of radial stress ($\sigma_{r,60°}$). The compressive deformation moduli have been measured from the tangent at about 40-50% of the peak stress.

Figures 5.3 and 5.4 show the direction of compressive elastic modulus (E_c) under different β angles of the transverse isotropic plane (bedding plane). The test results indicate that the compressive elastic modulus (E_c) increases with increasing the angle $\beta$, as shown in Figure 5.5(a). The Poisson's ratio under compression tends to decrease with increasing angle β, as shown in Figure 5.5(b). The results of tensile strength will be shown in the results under biaxial stress state.
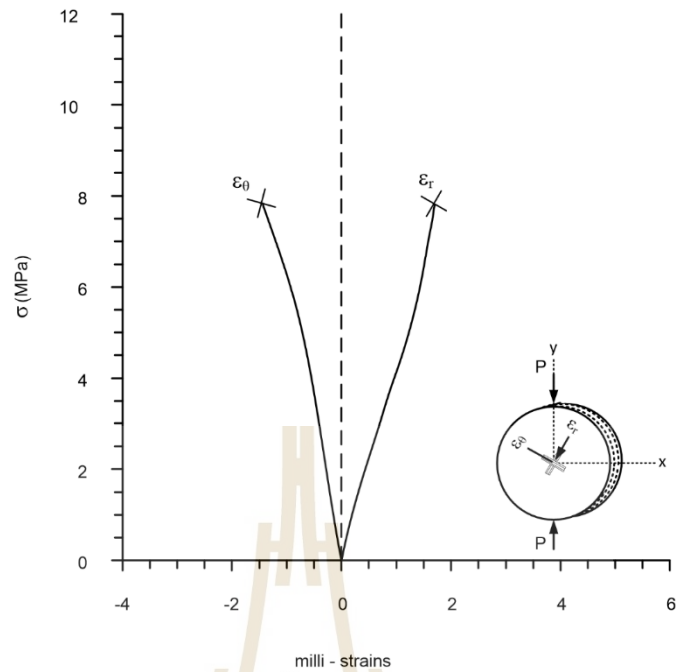
Figure 5.1 Stress-strain curve from uniaxial stress direction for bedding planes normal to core axis.
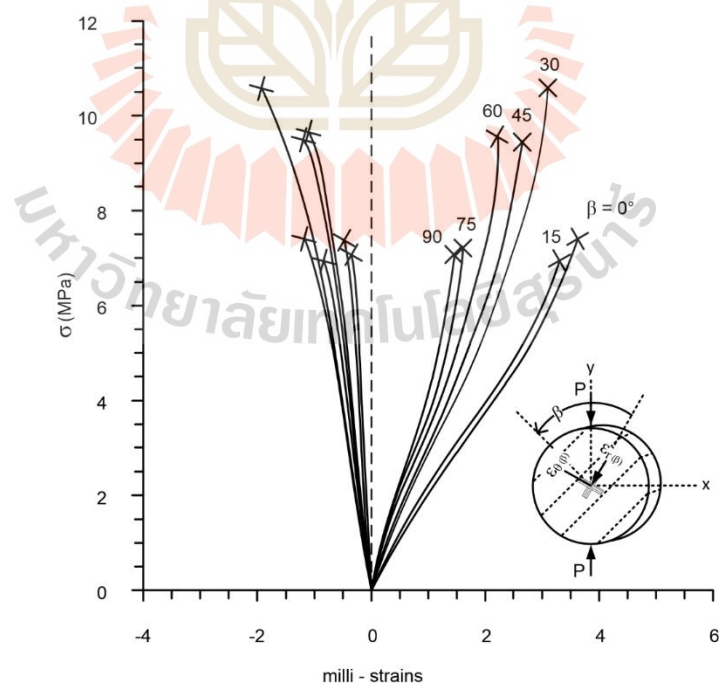
Figure 5.2 Stress-strain curves from uniaxial stress direction for bedding planes parallel to core axis with angle β varying from 0 to 90 degrees.
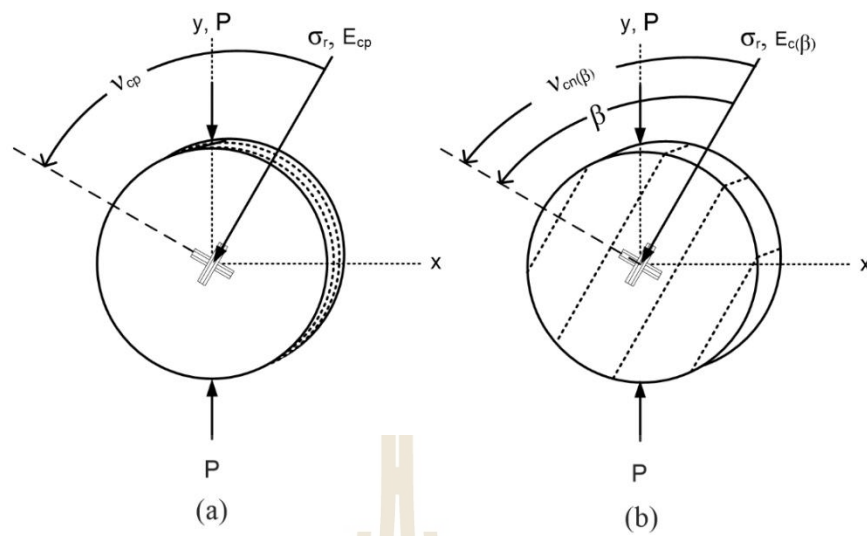
Figure 5.3 Directions to measure elastic moduli under uniaxial stress direction for bedding planes normal (a) and parallel (b) to core axis.
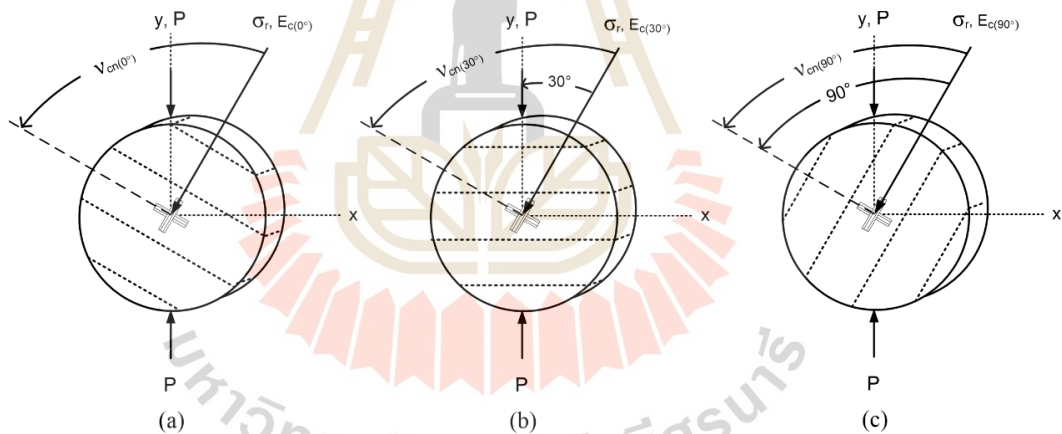
Figure 5.4 Directions to measure elastic moduli under uniaxial stress direction.
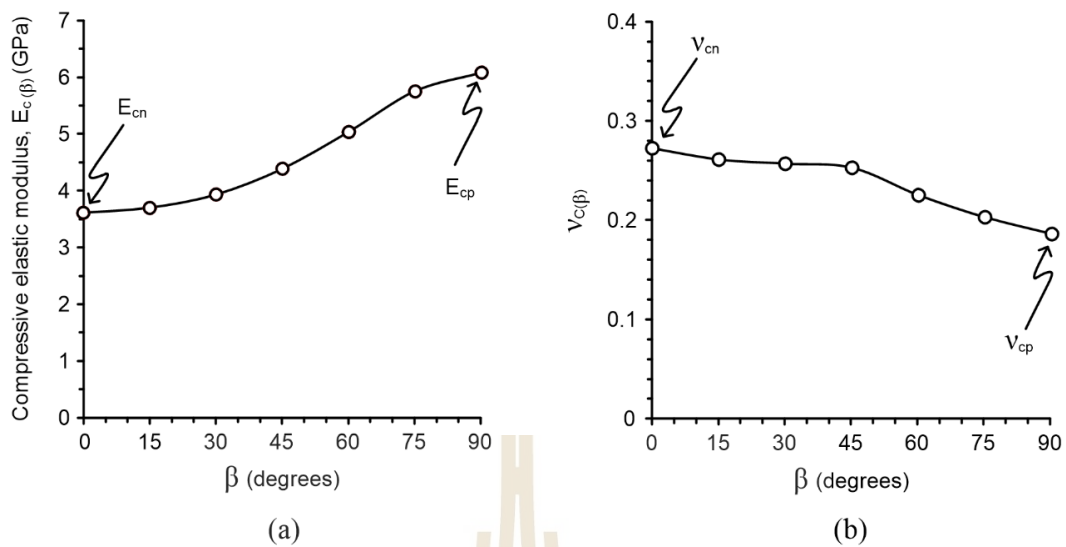
Figure 5.5 Compressive elastic moduli (E_c) and Poisson's ratios (v_c) under angle β varying from 0 to 90 degrees.

5.3 Test results under biaxial stress state

Figures 5.6 and 5.7 show the tensile stress-strain curves from start loading to failure under biaxial stress condition for specimens with bedding planes normal and parallel to the core axis. They are presented in the forms of loci of tensile strains (ε_t) and compressive strains (ε_c) as a function of tensile (σ_t) and compressive stress (σ_c). The results indicate the maximum tensile strength is 4.0 MPa for β = 0° (bedding planes normal to loading direction), and deceases to the minimum of 2.90 MPa for β = 90° (bedding planes parallel to loading direction). The tensile strength of specimen with bedding planes normal to core axis is 4.0 MPa.

The tensile strength decreases with increasing angle β, as shown in Figure 5.8. The direction of elastic moduli and Poisson's ratio under different β angles of the transverse isotropic plane (bedding plane) under biaxial stress state, is shown in Figure 5.9(a). The tensile elastic moduli decrease while the Poisson's ratio under tension increases with increasing angle β, as shown in Figures 5.9(b) and 5.10, respectively. Table 5.1 summarizes the elastic parameters under compression and tension. The strength results are given in Tables 5.2.
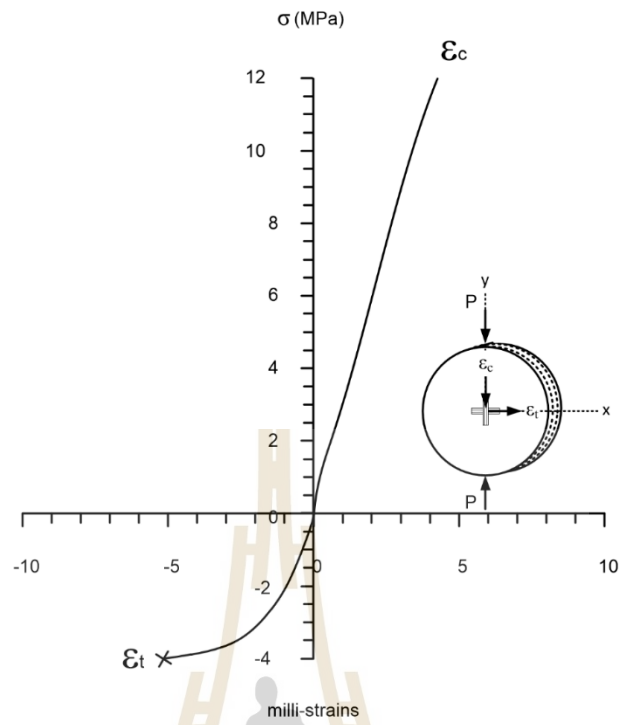
Figure 5.6 Stress-strain curve from biaxial stress state for bedding planes normal to core axis.
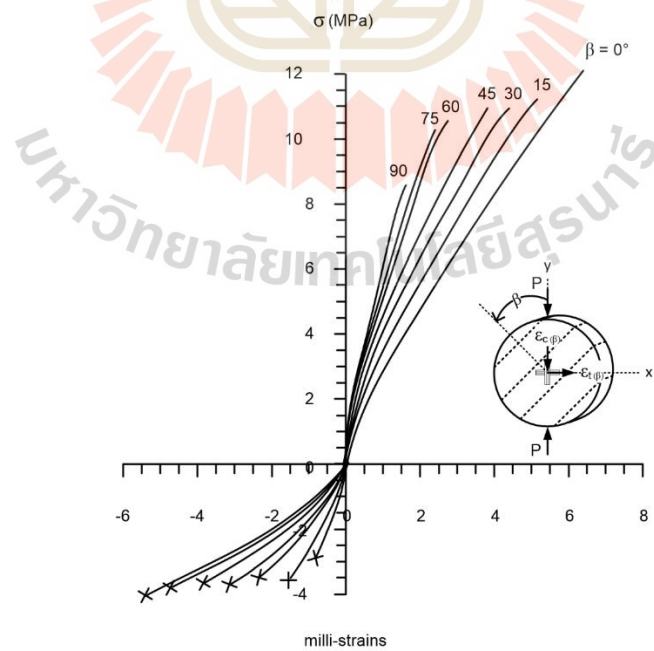
Figure 5.7 Stress-strain curves from biaxial stress state for bedding planes parallel to core axis.
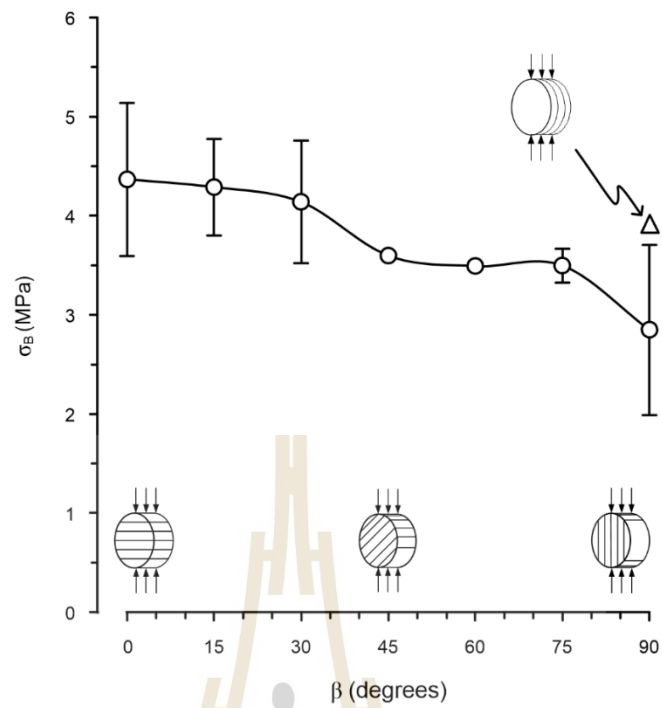
Figure 5.8 Brazilian tensile strength (σ_B), as a function of angle β.
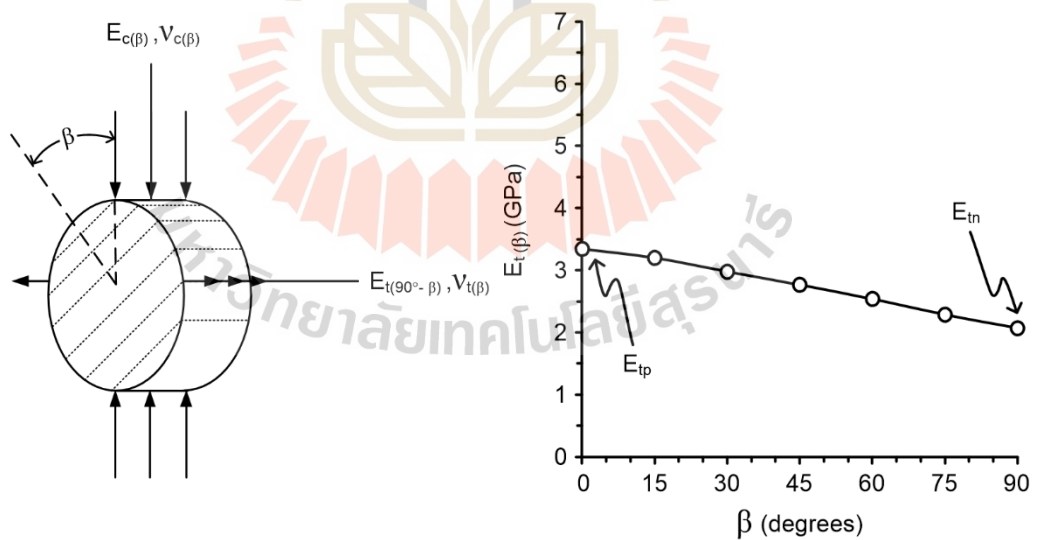
Figure 5.9 Direction of elastic moduli and Poisson's ratio under biaxial stress state (a), and variation of tensile elastic modulus (E_t) under different β angles (b).
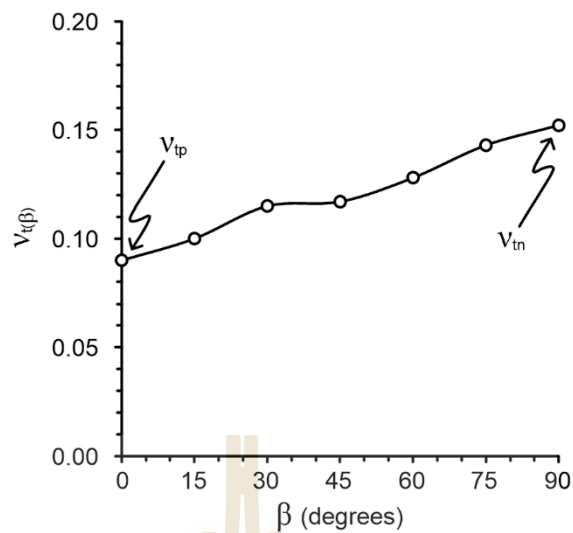
Figure 5.10 Poisson's ratios under tension (ν_t) for angle β varying from 0 to 90 degrees.

Table 5.1 Elastic parameters under compression and tension of sandstone specimens under all test conditions.

Bed orientation		Uniaxial stress state				Biaxial stress state			
Core axis	β (degrees)	E_{cp} (GPa)	E_{cn} (GPa)	$E_{c(\beta)}$ (GPa)	$\nu_{c(\beta)}$	E_{tp} (GPa)	E_{tn} (GPa)	$E_{t(\beta)}$ (GPa)	$\nu_{t(\beta)}$
Normal to core axis	-	6.06	-	-	0.19	3.42	-	-	0.09
Parallel to core axis	0	-	3.61	-	0.27	3.34	-	-	0.09
	15	-	-	3.70	0.26	-	-	3.21	0.10
	30	-	-	3.94	0.26	-	-	2.95	0.12
	45	-	-	4.39	0.25	-	-	2.85	0.12
	60	-	-	5.04	0.22	-	-	2.53	0.13
	75	-	-	5.75	0.20	-	-	2.29	0.14
	90	6.08	-	-	0.19	-	2.06	-	0.15

Table 5.2 Tensile strengths of sandstone specimens measured from biaxial testing.

Bed orientation		Biaxial stress state
Core axis	β (degrees)	σ_B (MPa)
Normal to core axis	-	4.0
Parallel to core axis	0	4.0
	15	3.7
	30	3.6
	45	3.6
	60	3.5
	75	3.4
	90	2.9

5.4   Mode of failure

Figure 5.11 shows post-test specimens tested to measure compressive elastic modulus and Poisson's ratio under different angles β measured from the gage direction. Tensile fractures are induced in all specimens. They cut through the bedding planes.

The post-test specimens under biaxial stress are shown in Figure 5.12. Here, angle β is measured from the loading direction which is the same as strain gage direction. The tensile fracture is induced in all specimens. They are cut through bedding planes for the cases when 0° $\leq$ β $\leq$ 60°. For β = 75° and 90°, the fracture is induced along the bedding planes.

Figure 5.11 Post-test specimens under uniaxial stress direction: (a) β = 0°, (b) β = 15°, (c) β = 30°, (d) β = 45°, (e) β = 60°, (f) β = 75° and (g) β = 90°.
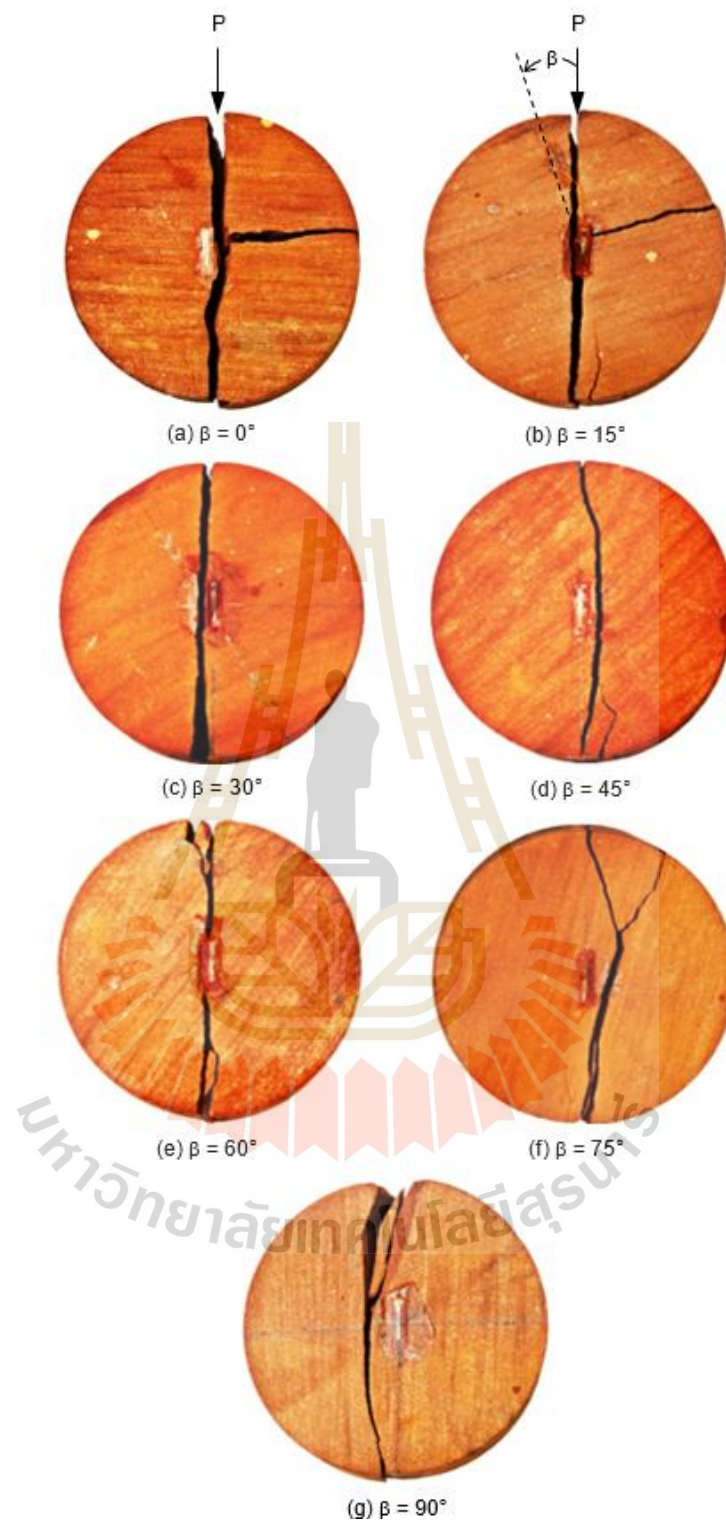
Figure 5.12 Post-test specimens under biaxial stress state: (a) β = 0°, (b) β = 15°,
(c) β = 30°, (d) β = 45°, (e) β = 60°, (f) β = 75° and (g) β = 90°.

CHAPTER VI
ANALYSIS OF TEST RESULTS

6.1 Introduction

The objective of this chapter is to mathematically define the transverse isotropic sandstone specimens. Tensile strength, compressive and tensile elastic parameters, and degrees of anisotropy as a function of bedding plane orientations are analyzed.

6.2 Transversely isotropy effect on tensile strength

The tensile strength of Phu Phan sandstone specimens decreases as bedding planes dip away from the loading direction, as shown in Figure 6.1. This is because the tensile cracks occur easily along with the seam layer of rock structure, especially when angle β = 90°. The tensile strength of sandstone obtained elsewhere is also compared in Figure 6.2. Sandstone from this study tends to show lower tensile strength compared to those from other researchers. Tensile strength of this study is about 69, 54, 40, and 25 percent lower than those of Tavallali and Vervoort. (2010), Khanlari et al. (2015), Khanlari et al. (2015), and Zhang et al. (2016). This may be due to the mineral compositions and density of Tavallali and Vervoort. (2010) and Khanlari et al. (2015) are 2.62 and 2.64 g/cm^3, and about 2.27-2.65 g/cm^3 by Khanlari et al. (2015) which are higher than of Phu Phan sandstone in this study. The maximum tensile strength is gradually reduced to the minimum tensile strength of about 74, 63, 69, 63, and 65 percent, respectively. This agrees well with the results obtained from other researchers.

Variation of the tensile strengths with bedding plane orientations can be best represented by linear equation, as follows:

$$\sigma_B = 4.490 - 0.017\beta \quad \text{(MPa)} \tag{6.1}$$

where σ_B is Brazilian tensile strength and angle β is the angle between loading direction and the normal to bedding planes. Good correlations are obtained ($R^2 > 0.9$).
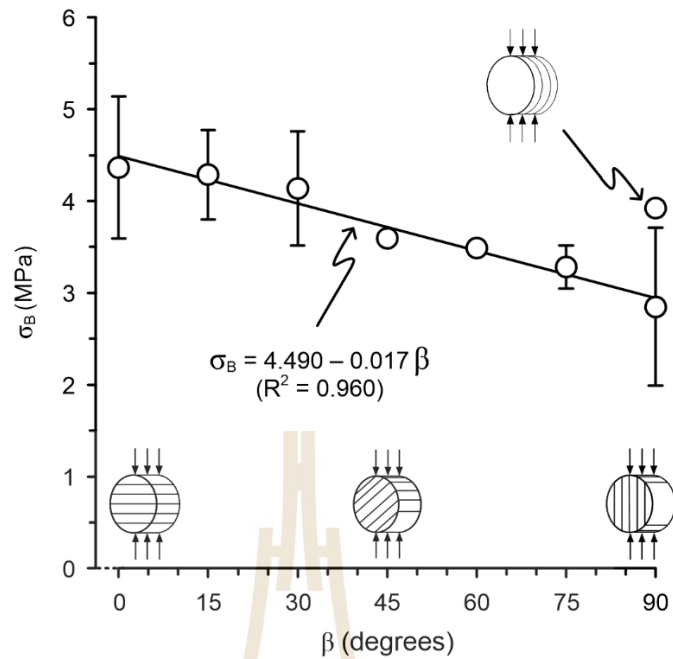
Figure 6.1 Relationship between Brazilian tensile strength (σ_B) and angle β of Phu Phan sandstone.
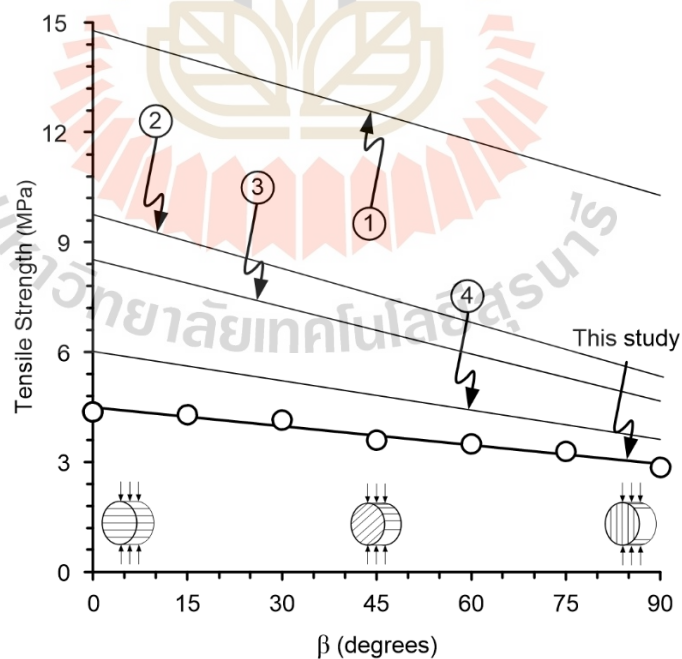
Figure 6.2 Relationship between tensile strength (σ_B) and angle β of Phu Phan sandstone as compared to those of (1) Tavallali and Vervoort. (2010), (2) Khanlari et al. (2015), (3) Khanlari et al. (2015), and (4) Zhang et al. (2016).

6.3 Transverse isotropy effect on elastic parameters

The compressive elastic modulus increases and the tensile elastic modulus decreases as increasing angle β. The results suggest that the tensile elastic modulus is lower than the compressive elastic modulus. This is because the effort required to dilate the pore spaces and fissures in the rocks under compression is higher than that under tension. The results obtained here show the tensile elastic modulus of about 56 percent lower than that of the compressive elastic modulus. This agrees reasonably well with the results obtained be Jianhong et al. (2008), Fuenkajorn and Klanphumeesri (2010), and Patel and Martin (2018), who find that tensile elastic moduli obtained by direct tension test is about 71, 42, and 65 percent of compressive elastic moduli obtained by uniaxial compression test.

These elastic moduli tend to vary linearly with angle β. The empirical constants in the linear equations are shown in Figure 6.3, with the correlation coefficients of greater than 0.9.

$$E_{C(\beta)} = 3.293 + 0.030\,\beta \qquad \text{(GPa)} \tag{6.2}$$

$$E_{T(\beta)} = 3.392 - 0.015\,\beta \qquad \text{(GPa)} \tag{6.3}$$

where $E_{C(\beta)}$ is compressive elastic modulus and $E_{T(\beta)}$ is tensile elastic modulus.

The relationship between Poisson's ratios under compression $v_{C(\beta)}$ and under tension $v_{T(\beta)}$ and bedding plane orientations is shown in Figure 6.4. The Poisson's ratio under compression decreases and Poisson's ratio under tension increases with increasing angle β. This is probably due to that the radial strain laterally dilates more than those under tangential strain. The linear relation between the $v_{C(\beta)}$ and $v_{T(\beta)}$ and angle β can be best represented by:

$$v_{C(\beta)} = 0.279 - 0.001\,\beta \qquad \text{(GPa)} \tag{6.4}$$

$$v_{T(\beta)} = 0.093 + 0.0006\,\beta \qquad \text{(GPa)} \tag{6.5}$$

The correlation coefficients (R^2) are 0.952 and 0.996, respectively.
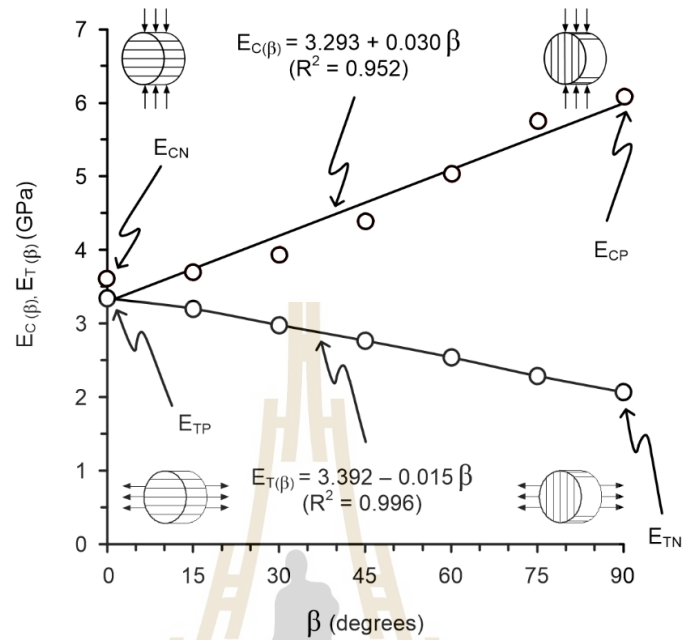
Figure 6.3 Relationship between elastic moduli and angle β of Phu Phan sandstone.
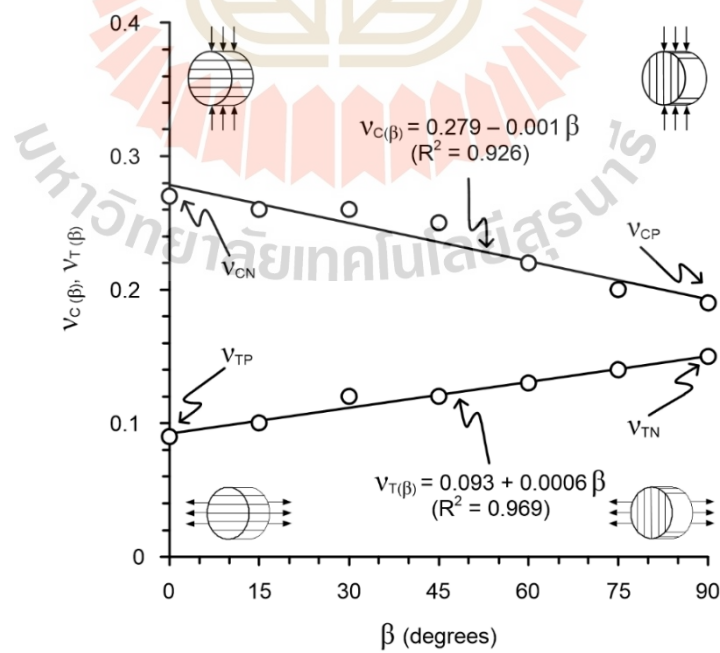
Figure 6.4 Relationship between Poisson's ratio (σ_B) and angle β of Phu Phan sandstone.

6.4   Degrees of rock anisotropy

Several investigators (Ramamurthy, 1993; Niandou et al., 1997; Hakala et al., 2007; Ismael et al., 2014; Abbass et al., 2019; You et al., 2021) have determined the degrees of rock anisotropy and rock classes using the ratios of the maximum-to-minimum strength and maximum-to-minimum elastic moduli on the plane of transverse isotropy.

The higher values of $\sigma_{max}/\sigma_{min}$ and E_{max}/E_{min} ratios indicate the stronger degree of anisotropy. Based on the test results reported in previous chapter, the $\sigma_{max}/\sigma_{min}$ and E_{max}/E_{min} ratios of Phu Phan sandstone have been calculated. Figure 6.5 plots the maximum tensile strength (σ_{max}) in terms of the minimum tensile strength (σ_{min}) to determine the degree of anisotropy. Table 6.1 gives their numerical values. The degrees of anisotropy of various rocks obtained elsewhere are also compared in the figure. This study tends to show lower degree of anisotropy compared to the foliation rocks. The results show that schist, slate, and gneiss specimen show higher degree of anisotropy than shale and sandstone specimens. This may be due to types of rocks. The metamorphic rock tents to show higher degree of anisotropy than the sedimentary rock.
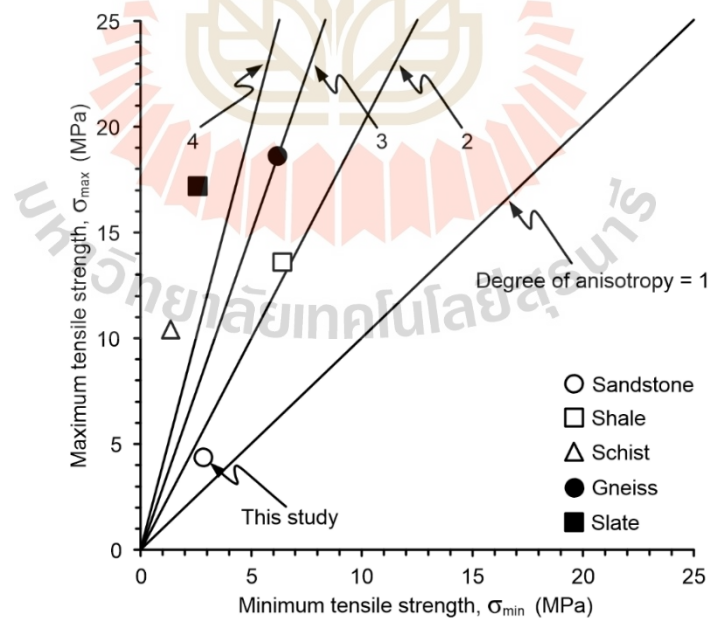
Figure 6.5 Relationship between maximum tensile strength (σ_{max}) and minimum tensile strength (σ_{min}) from sandstone (this study), shale (Park and Min, 2015),

schist (Park and Min, 2015), gneiss (Park and Min, 2015), and slate (Han et al., 2020).

The degree of anisotropy in terms of the maximum-to-minimum elastic moduli under compression and tension is shown in Figure 6.6. The results indicate that degree of anisotropy in terms of elastic moduli under compression and tension are similar: 1.68 and 1.62, respectively.

Table 6.1 Maximum-to-minimum strength on degree of anisotropy.

Type of rock	Tensile strength (MPa)		Degree of anisotropy	Resource
	Maximum strength, σ_{max}	Minimum strength, σ_{min}		
Sandstone	4.37	2.85	1.53	This study
Shale	13.60	6.40	2.13	Park and Min. (2015)
Schist	17.20	2.60	6.62	Park and Min. (2015)
Gneiss	18.60	6.20	3.00	Tavallali and Vervoort. (2010)
Slate	10.44	1.38	7.57	Han et al. (2020)
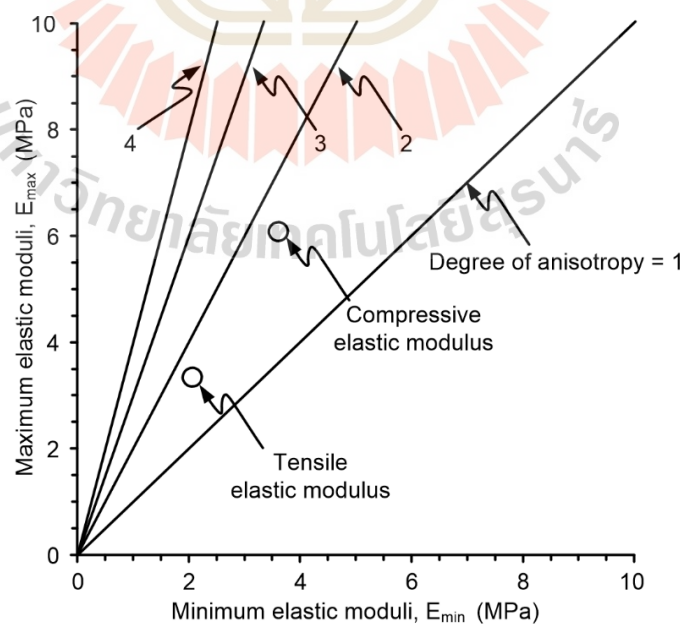
Figure 6.6 Relationship between maximum elastic moduli (E_{max}) and minimum elastic moduli (E_{min}) under compression and tension of this study.

Table 6.2 Maximum-to-minimum elastic moduli on degree of anisotropy.

Elastic moduli			Degree of anisotropy
Compressive elastic moduli, (GPa)	$E_{C,max}$	6.08	1.68
	$E_{C,min}$	3.61	
Tensile elastic moduli, (GPa)	$E_{T,max}$	3.34	1.62
	$E_{T,min}$	2.06	

CHAPTER VII
NUMERICAL SIMULATIONS

7.1   Introduction

This chapter describes the results of finite element analyses by using Phase2 under plane strain analysis (Rocscience, 2016). The objective of numerical simulations is to determine the effect of transverse isotropy on stress distribution and deformation behavior of Phu Phan sandstone. Phase2 is used to determine on horizontal stress distribution and horizontal displacement under various bedding plane orientations from 0, 15, 30, 45, 60, 75, and 90 degrees. The results can help explain the evolution of the strengths and displacements as measured from the testing.

7.2   Numerical modelling (Phase2 program)

Phase2 is used to simulate horizontal stress distribution and horizontal displacement of transverse isotropic specimens under various bedding planes from 0 to 90 degrees with 15 degrees intervals. It can be used to explain deformation behavior of transverse isotropy on sandstone. Phase2 is a finite element analysis under two dimensions. To cover boundary of disk, about 700 triangle elements have been constructed. The disk boundary conditions can move freely in x and y axes. Line load are applied along y-axis to obtain simulation results. Shape, dimensions, and model for simulation of specimen are identical to those used in the test, as shown in Figure 7.1.

7.3   Property parameters used in numerical modelling

The material parameters of Phase2 are defined as transverse isotropic elastic properties based on Mohr-Coulomb material. The material parameters are divided into two portions elastic properties and strength parameters. The elastic properties are obtained from laboratory, including shear modulus (G), elastic modulus in parallel to bedding plane (E_1), elastic modulus in normal to bedding plane (E_2), Poisson's ratio in parallel to bedding plane (v_{1z}), and Poisson's ratio in normal to bedding plane (v_{12}). The angle β is measured between x-axis and direction of E1, as shown in Figure 7.2. The strength parameters are obtained from both laboratories is tensile strength and this study are friction angle and cohesion. The simulations use a load line of 0.47 MN,

which this value is calibrated to provide the tensile strength close to that of laboratory testing at zero degrees. Table 7.1 shows the parameters used in Phase2 simulations.
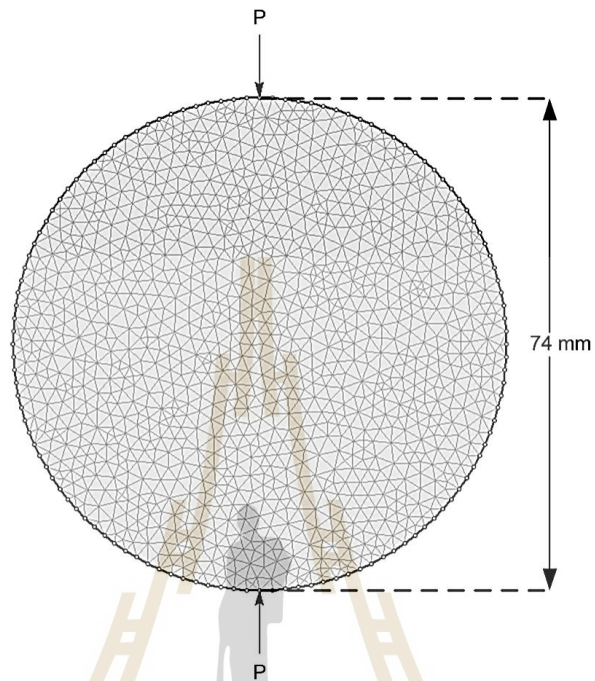
Figure 7.1 Mesh and boundary conditions used for finite difference analysis of Brazilian tension test. It represents the 74 mm disk diameter. Arrow (P) indicates the direction of load.
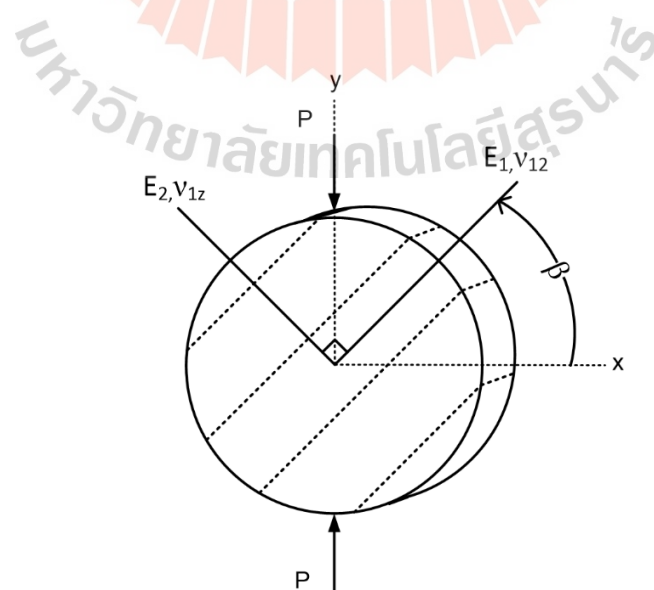
Figure 7.2 Directions to measure angle β under material parameter by using Phase2.

Table 7.1 Material parameters used for numerical modeling.

Parameters		Values	Sources
Elastic properties	Shear modulus, G (GPa)	1.69	Laboratory test
	Elastic modulus, E_1 (GPa)	6.08	
	Possion' ration, ν_{12}	0.27	
	Elastic modulus, E_2 (GPa)	3.61	
	Possion' ration, ν_{1z}	0.19	
	Tensile strength (MPa)	4.00	
Strength paramet	Friction angle (degrees)	41	This study
	Cohesion (MPa)	12.95	
	Line load (MN)	0.47	

7.4   Numerical results

Numerical results show the effect of transverse isotropy on horizontal stress distributions and horizontal displacements. Figure 7.3 shows horizontal displacements vector under various angles β. All specimens show an initial crack around center of disk and extending along bedding planes. The results of horizontal displacements indicate that the deformation vector for β = 0° gradually reduce to β = 90° which similar to the laboratory test.

Normalized horizontal stress distributions under various angles β are shown in Figure 7.4. The figure shows that maximum tensile stress occurs at the center point of disk and the compressive stress concentration around the contact zones of disk (the upper and lower zones). Phase2 program can be used to measure the maximum stress on the specimen for each bedding plane orientation. This agrees well with the results given by Hondron (1959) and Ma and Hung (2008), as shown in Figure 7.5. The results indicate that the normalized horizontal stress distribution contours show the maximum horizontal stress occurs at the center point of disk when β = 0° and gradually reduces to β = 90°, as shown in Figure 7.4. It is because the deformations at β = 0° are higher than those of β = 90°.

7.5   Discussions of numerical results

The numerical simulations indicate that the tensile strength decreases with increasing bedding plane orientations. The numerical simulations show the tensile strength higher than the laboratory tests about 1.2 times under the same condition, as shown in Figure 7.6. This is because the numerical simulation is simulated in

2-dimension which is different from the experimental laboratory and the effect of inclusions such as clay minerals, quartz, and calcite on sandstone specimens is not considered in the numerical simulations. The tensile strength is sensitive to bedding plane orientations. The observations are consistent with those of Tan et al. (2015). Table 7.2 gives tensile strengths obtained from numerical simulations and laboratory tests.
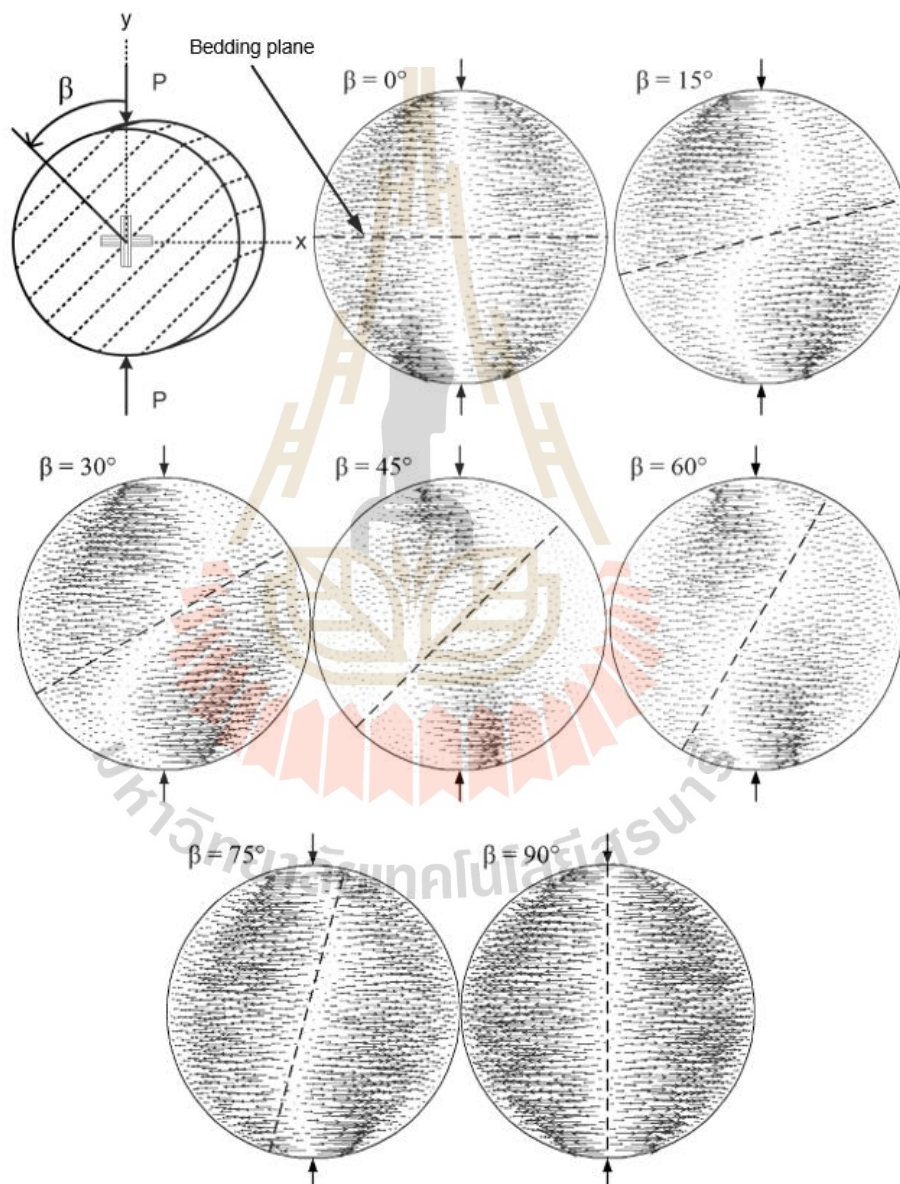
Figure 7.3 Horizontal displacements vectors at various angle β.
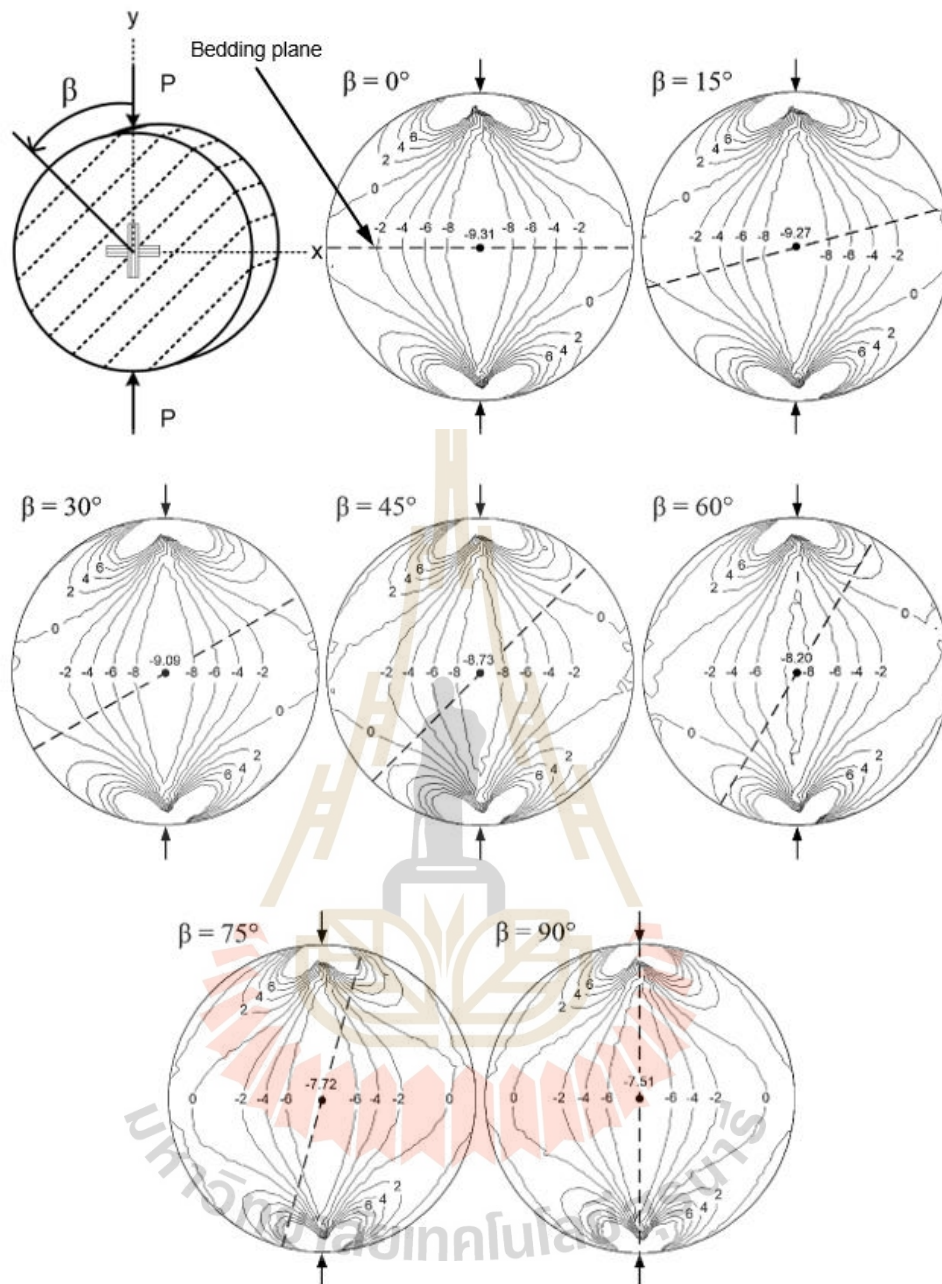
Figure 7.4 Normalized horizontal stress(σ_{xx}/P) distribution at various angles β. Arrow indicates the direction of loading. P = 0.47 MN. σ_{xx}/P has unit of 1/m^2.
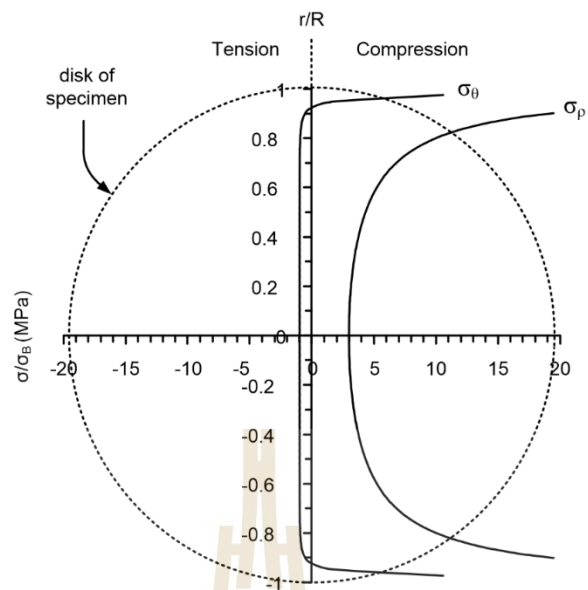
Figure 7.5 Radial and tangential stress distributions on disk of Brazilian tension test (Ma and Hung, 2008).
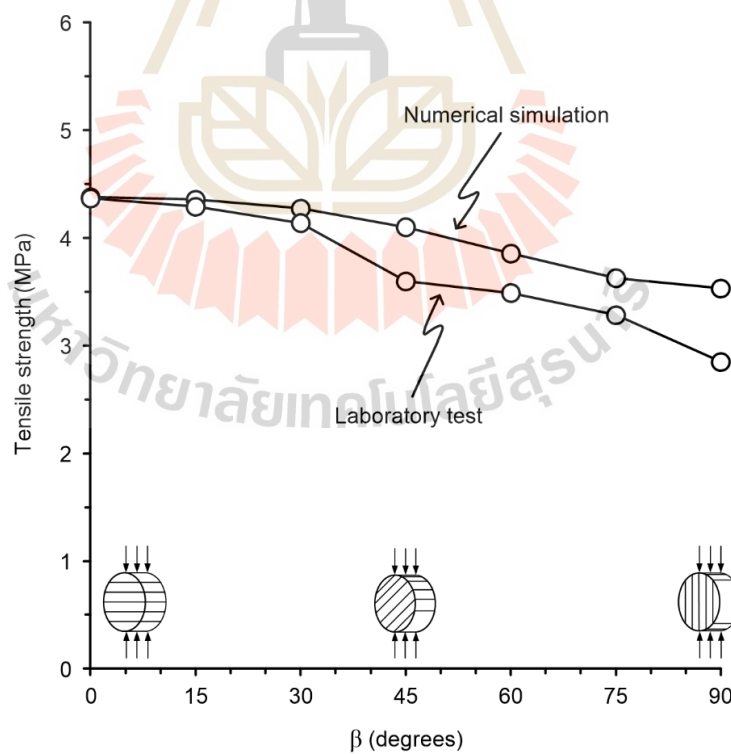
Figure 7.6 Comparison tensile strength between laboratory test and numerical simulations at center point of disk under various angles β.

Table 7.2 Tensile strength obtained from numerical simulations and laboratory tests.

β (degrees)	Tensile strengths (MPa)	
	Numerical simulations	Laboratory tests
0	4.38	4.37
15	4.35	4.29
30	4.27	4.14
45	4.10	3.60
60	3.86	3.49
75	3.63	3.29
90	3.53	2.85

CHAPTER VIII
DISCUSSIONS AND CONCLUSIONS

8.1   Introduction

Presented in this chapter is the compression of the results obtained here with those obtained elsewhere in terms of their anisotropy degrees, discussions of the research method, and results with respect to their adequacy and reliability are given. Conclusions draw from the research findings are presented.

8.2   Comparisons

Both tensile strength and deformability responses of the tested sandstone are sensitive to bedding (transversely isotropic) plane. Table 8.1 gives the maximum and minimum tensile strengths of various values obtained by other researchers. The degree of anisotropy of the Phu Phan tensile strength tends to be low as compared to those of other results. Figure 8.1 shows the bedding planes are well defined, as compared to other rocks tested elsewhere. It can be observed that sedimentary rocks and metamorphic rocks are sensitive to the transverse isotropy plane (bedding plane) while the maximum tensile strength depends on bonded particles and main compositions of each of the rock types including quartz, feldspar, mica, and clay minerals. It is a reason why the tensile strength and anisotropy degree of sedimentary rocks are lower than metamorphic rocks

The tensile elastic moduli obtained under biaxial stress state are lower than Chen et al. (1998) on bedded sandstone and Yun et al. (2012) on Zheng Tuanchong slate under same experimental, as shown in Figure 8.2. The results of this study and Chen et al. (1998) show similar trend under the same rock type while they are different from the results of Yun et al. (2012) on Zheng Tuanchong slate. The compressive elastic moduli obtained under uniaxial stress state show tend to be lower than Amadei (1996) on sandstone, Hakala et al. (2007) on Olkiluoto mica gneiss and Singkhiaw et al. (2021) on Phu Phan sandstone under uniaxial compression test, as shown in Figure 8.3. The results of this study show a similar trend to Amadei (1996) and Hakala et al. (2007) and give a close value to Singkhiaw et al. (2021) under same rock type. Consequently, the reliability of the test method proposed here is shown to be good under same rock

type. Tables 8.2 and 8.3 give the results of the tensile and compressive moduli of this study and other researchers, respectively.

The compressive elastic moduli are higher than the tensile elastic moduli. The Poisson's ratio under compression is higher than tension. This agrees reasonably well with the results obtained by Jianhong et al. (2008) who performed Brazilian tension tests and uniaxial compression tests on sandstone. The results agree with those of Haimson and Tharp (1974) and Fuenkajorn and Klanphumeesri (2010) who performed direct tension tests and uniaxial compression tests on sandstone. Table 8.4 gives the tensile (E_t) and compressive (E_c) modulus values of sandstone.
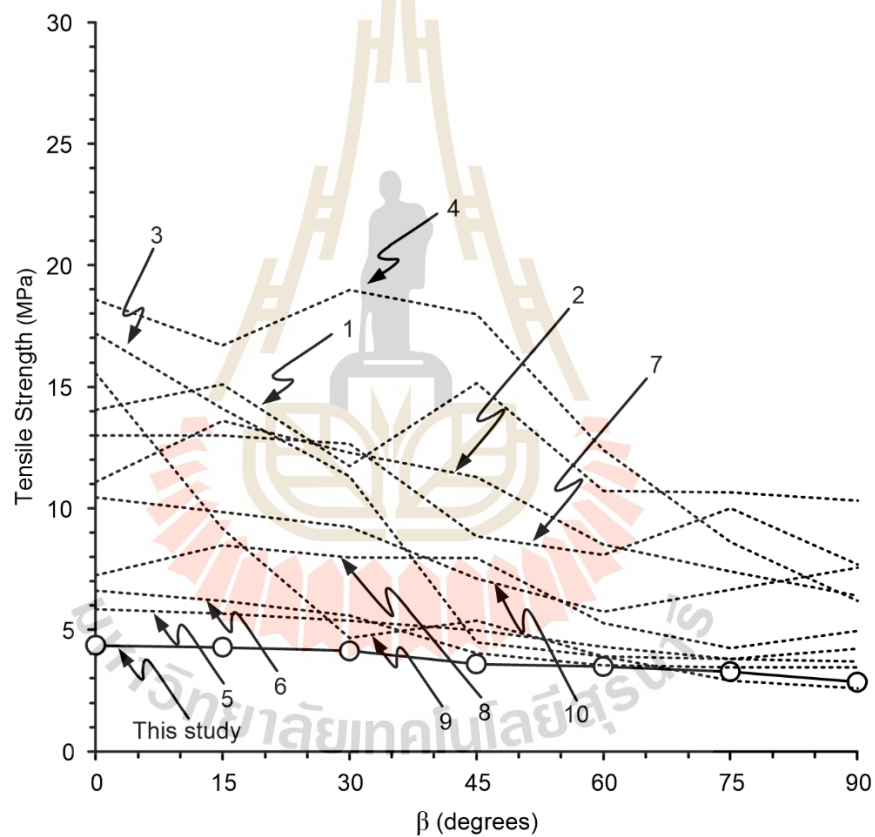
Figure 8.1 Tensile strength as a function of bedding plane orientations. (1) Tavallali and Vervoort. (2010) on Modave sandstone, (2) Park and Min (2015) on Boryeong shale, (3) Park and Min (2015) on Yeoncheon schist, (4) Park and Min (2015) on Asan gneiss, (5) Zhang et al. (2016) on Bedded sandstone, (6) Ma et al. (2018) on Longmaxi shale, (7) Yang et al. (2020) on Lushan shale, (8) Khanlari et al. (2015) on Laminated sandstone, (9) Tan et al. (2015) on Mosel slate, and (10) Han et al. (2020) on Muzhailing slate.

Numerical simulations show the horizontal displacement vector and horizontal stress to obtain the maximum tensile stress. The tensile strength and stress distributions are agreed well with laboratory results by Dan (2011), and Tan et al. (2015) who performed numerical simulations variety FLAC[3D] and UDEC. The horizontal stress distributions indicate the crack initiation around the center of disk. It agrees well with the results by Van De Steen et al. (2005), Zhu and Tang (2006), and Cai and Kaiser (2004) which different from Li and Wong (2013) and Markides and Kourkoulis (2012) who found that the crack initiation point did not occur away from the center of disk.

Table 8.1 Maximum and minimum tensile strength results of various types of rocks.

Type of rocks	Tensile strength (MPa)		Degree of anisotropy	Resources
	Maximum	Minimum		
Phu Phan sandstone	4.37	2.85	1.53	This study
Modave sandstone	15.13	10.33	1.47	Tavallali and Vervoort. (2010)
Boryeong shale	13.60	6.40	2.13	Park and Min (2015)
Yeoncheon schist	17.20	2.60	6.62	
Asan gneiss	19.00	6.20	3.06	
Bedded sandstone	5.85	3.70	1.58	Zhang et al. (2016)
Longmaxi shale	6.61	3.47	1.91	Ma et al. (2018)
Lushan shale	12.99	7.69	1.69	Yang et al. (2020)
Laminated sandstone	8.48	4.24	2.00	Khanlari et al. (2015)
Mosel slate	15.56	3.80	4.09	Tan et al. (2015)
Muzhailing slate	10.44	5.75	1.82	Han et al. (2020)
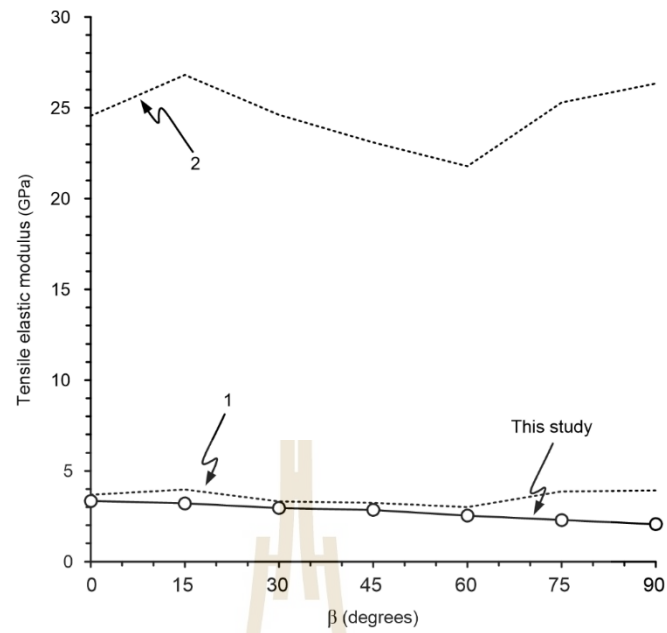
Figure 8.2 Tensile elastic moduli as a function of bedding plane orientations.
(1) Chen et al. (1998) on bedded sandstone and (2) Yun et al. (2012)
on Zheng Tuanchong slate.
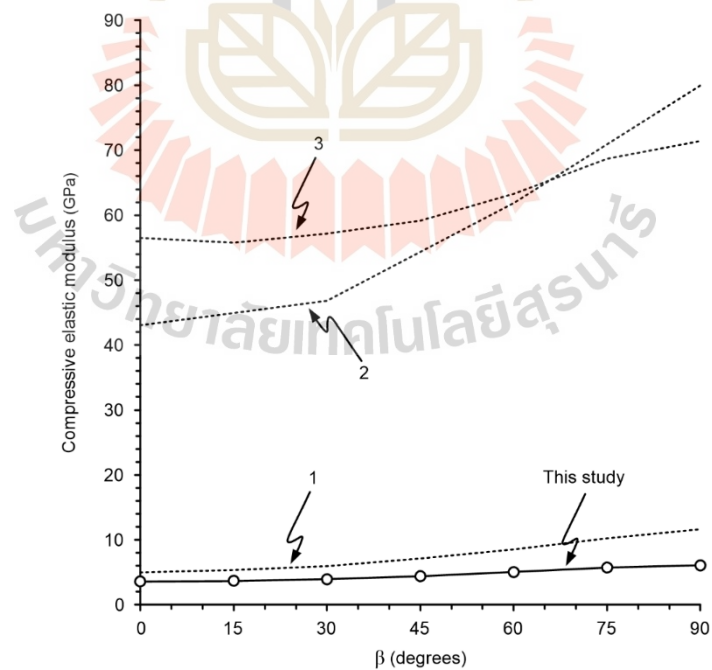
Figure 8.2 Tensile elastic moduli as a function of bedding plane orientations.
(1) Chen et al. (1998) on bedded sandstone and (2) Yun et al. (2012)
on Zheng Tuanchong slate.
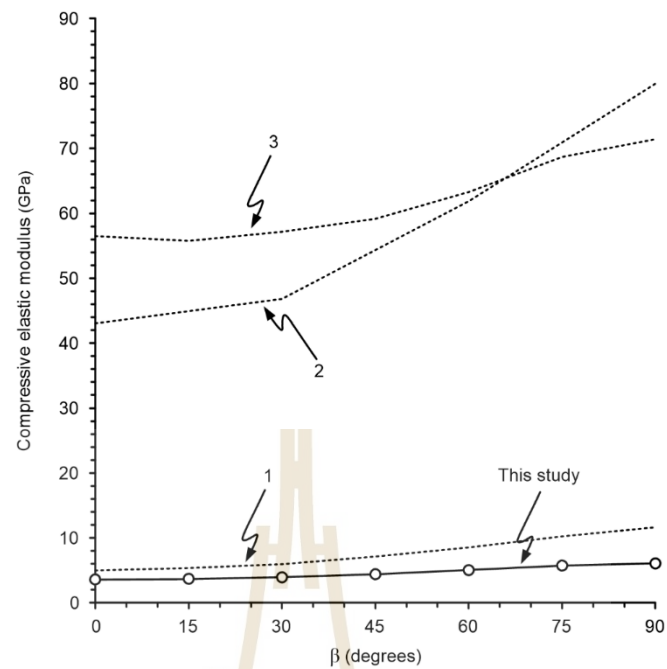
Figure 8.3 Compressive elastic moduli as a function of bedding plane orientations.
(1) Singkhiaw et al. (2021) on Phu Phan sandstone, (2) Amadei (1996) on
bedded sandstone, and (3) Hakala et al. (2007) on Olkiluoto mica gneiss.

Table 8.2 Tensile elastic moduli of various types of rocks.

β (degrees)	Tensile elastic modulus (GPa)		
	This study	Chen et al. (1998)	Yun et al. (2012)
	Phu Phan sandstone	Bedded sandstone	Zheng Tuanchong slate
0	3.34	3.67	24.6
15	3.21	3.96	26.8
30	2.95	3.32	24.6
45	2.85	3.24	23.1
60	2.53	3.00	21.8
75	2.29	3.86	25.3
90	2.06	3.90	26.3

Table 8.3 Maximum and minimum tensile strengths of various types of rocks.

β (degrees)	Compressive elastic modulus (GPa)			
	This study	Amadei (1996)	Hakala et al. (2007)	Singkhiaw et al. (2021)
	Phu Phan sandstone	Bedded sandstone	Olkiluoto mica gneiss	Phu Phan sandstone
0	3.61	43.0	56.5	5.0
15	3.7	-	55.8	5.4
30	3.94	46.8	57.1	6.0
45	4.39	-	59.2	7.1
60	5.04	61.9	63.3	8.5
75	5.75	-	68.7	10.2
90	6.08	80.0	71.4	11.6

Table 8.4 Tensile (E_t) and compressive (E_c) moduli values of sandstone.

Type of rocks	E_t (GPa)	E_c (Gpa)	E_t/E_c (%)	Resources
Phu Phan sandstone	2.06	6.08	33.9	This study
Arizona sandstone	11.7	45.5	25.7	Haimson and Tharp (1974)
Berea sandstone	4.1	23.4	17.5	
Millsap sandstone	0.7	13.1	5.3	
Tennessee sandstone	1.4	16.5	8.5	
Russian sandstone	11.7	57.2	20.5	
Sandstone	7.1	10.0	70.9	Jianhong et al. (2008)
Phu Phan sandstone	6.7	16.2	41.4	Fuenkajorn and Klanphumeesri (2011)

8.3   Discussions

Admittedly the number of rock specimens used here tends to be limited. This is primarily due to the differently in same properties. The results, nevertheless, tend to show clear trends of transverse isotropy rock in the terms of the strength and elastic parameters. Under Brazilian tension test, the designed strain gage directions are aimed at obtaining the compressive and tensile elastic parameters and hence reveals the strength and elastic parameters in terms of the transverse isotropy effect on Phu Phan sandstone.

It is found here that the tensile strength decreases with increasing bedding plane orientations while the minimum tensile strength occurs when the normal bedding planes make an angle (β) of 90 degrees with the loading direction. This agrees with the test results obtained by Tavallali and Vervoort. (2010) on Modave sandstone, Park and Min (2015) on Boryeong shale, Yeoncheon schist, and Asan gneiss, Zhang et al. (2016) on bedded sandstone, Ma et al. (2018) on Longmaxi shale, and Yang et al. (2020) on Lushan shale. This behavior may be true for other rock types.

Brazilian tension test under uniaxial and biaxial stress proposed here to reveal the compressive and tensile elastic parameters are not equal, which is different from the results are given by Amadei (1996). As a result, the compressive elastic parameters are higher than those tensile elastic parameters, which shows a similar trend from Fuenkajorn and Klanphumeesri (2010), Jianhong et al. (2009), and Patel and Martin (2018).

Empirical equations in linear form can well describe the Phu Phan sandstone tensile strength, elastic moduli, and Poisson's ratio for all bedding plane orientations and can be used for sedimentary rocks because when they observed the comparison, sedimentary rocks show the similar value with this study.

The Brazilian tension test is simple to prepare specimens and the test method under compression and tension stress on parallel and normal with loading directions, respectively. The bi-axial stress is an advantage because helpful when simulating uniaxial and biaxial stress states in this test. Although tensile strength can be obtained from several tests such as the direct tension test, bending test, Brazilian tension test, and ring test. Direct tension tests and bending tests are difficult to prepare specimens and test methods. Ring test is a similar method to Brazilian tension test but gives the highest tensile strength in situ condition. This is a reason why the Brazilian tension test was used here.

8.4 Conclusions

Conclusion drawn from this study can be summarized as follows:

1) The variation of tensile strength with bedding plane orientations shows a linear relation where the maximum tensile strength of 4.37 MPa when loading is perpendicular to the bedding (anisotropic) planes and the minimum tensile strength of 2.85 MPa when loading is parallel to the bedding (anisotropic) planes

2) The measured compressive and tensile elastic modulus varies from 6.08 to 3.61 GPa, and 3.34 to 2.06, respectively, depending on the orientations of bedding planes. The results show transversely isotropic properties where the elastic modulus

in the direction parallel to the bedding planes is greater than that normal to the bedding planes.

3) The measured Poisson's ratios of compressive and tensile vary from 0.27 to 0.19 and 0.15 to 0.09, respectively, depending on the bedding orientations. The Poisson's ratio on the plane parallel to the bedding plane is lower than those on the plane normal to the bedding plane.

4) Under Brazilian tension tests, compressive and tensile elastic modulus are not equal and tend to be sensitive to the transverse isotropic plane (bedding plane).

5) Numerical simulations demonstrate the tensile strength and deformation behavior under bedding plane orientations (transverse isotropic rock). It can prove tensile strength and deformability highly sensitive to transverse isotropy plane (bedding plane).

8.5   Recommendations for future studies

1) Larger specimen numbers and sizes and dry-wet conditions may be used to enhance the understanding of the anisotropic responses of the results.

2) More diverse rock types and mineral compositions are desirable in order to truly assess all factors of the effect of transversely isotropy rocks.

3) Other tensile testing methods should be studied to compare and approve the test results in this study, such as bending tests, etc.

REFERENCES

Abbass, H. A., Mohamed, Z., & Yasir, S. F. (2019). A review of methods, techniques and approaches on investigation of rock anisotropy. *In AIP Conference Proceedings*. 2020(1): 020012).

Amadei, B. (1996). Importance of anisotropy when estimating and measuring in situ stresses in rock. *International Journal of Rock Mechanics and Mining Sciences & Geomechanics Abstracts*. 33(3): 293-325.

ASTM D3967-16. (2016). *Standard Test Method for Splitting Tensile Strength of Intact Rock Core Specimens*. Annual Book of ASTM Standards. West Conshohocken, PA.

Cai, M., and Kaiser, P. K. (2004). Numerical Simulation of The Brazilian Test and The Tensile Strength of Anisotropic Rocks and Rocks with Pre-Existing Cracks. *International Journal of Rock Mechanics and Mining Sciences*. 41: 478-483.

Chen, C. S., and Hsu, S. C. (2001). Measurement of Indirect Tensile Strength of Anisotropic Rocks by the Ring Test. *Rock Mechanics and Rock Engineering*. 34(4): 293-321.

Chen, C.-S., Pan, E., and Amadei, B. (1998). Determination of deformability and tensile strength of anisotropic rock using Brazilian tests. *International Journal of Rock Mechanics and Mining Sciences*. 35(1): 43-61.

Cheng, C., Li, X., and Qian, H. (2017). Anisotropic failure strength of shale with increasing confinement: behaviors, factors and mechanism. *Materials*. 10(11): 1310.

Dan, D. (2011). Brazilian test on anisotropic rocks-laboratory experiment, numerical simulation and interpretation. *Numerical simulation and interpretation*. Institut für Geotechnik, Freiberg.

Duveau, G., and Shao, J. F. (1998). A modified single plane of weakness theory for the failure of highly stratified rocks. *In International Journal of Rock Mechanics and Mining Sciences*. 6(35): 807-813.

Fuenkajorn, K. and Klanphumeesri, S. (2010). Direct tension tests of intact rocks using compression-to-tension load converter. *Engineering Journal of Research and Development*. 21(2): 51-57.

Haimson, B. C., and Tharp, T. M. (1974). Stresses Around Boreholes in Bilinear Elastic Rock. *Society of Petroleum Engineers Journal*. 14(02): 145-151.

.

Hakala, M., Kuula, H., and Hudson, J. A. (2007). Estimating the transversely isotropic elastic intact rock properties for in situ stress measurement data reduction: A case study of the Olkiluoto mica gneiss, Finland. *International Journal of Rock Mechanics and Mining Sciences*. 44(1): 14

Hakala, M., Kuula, H., and Hudson, J. A. (2007). Estimating the transversely isotropic elastic intact rock properties for in situ stress measurement data reduction: A case study of the Olkiluoto mica gneiss, Finland. *International Journal of Rock Mechanics and Mining Sciences*. 44(1): 14-46.

Han, W., Fuqiang, R., and Yuan, C. (2020). Effect of bedding angle on tunnel slate failure behavior under indirect tension. Geomatics, *Natural Hazards and Risk*. 11(1): 428-445.

Hondros, G. (1959). The evaluation of Poisson's ratio and the modulus of materials of a low tensile resistance by the Brazilian (indirect tensile) test with particular reference to concrete. *Australian Journal of Applied Science*. 10: 243-264.

Ismael, M. A., Imam, H. F., and El-Shayeb, Y. (2014). A simplified approach to directly consider intact rock anisotropy in Hoek–Brown failure criterion. *Journal of Rock Mechanics and Geotechnical Engineering*. 6(5): 486-492.

Jaeger JC, Cook NGW, Zimmerman R. (2007). *Fundamentals of rock mechanics*, 4th edn. Chapman and Hall, London. 475P

Jianhong, Y., Wu, F. Q., and Sun, J. Z. (2009). Estimation of the tensile elastic modulus using Brazilian disc by applying diametrically opposed concentrated loads. *International Journal of Rock Mechanics and Mining Sciences*. 46(3): 568-576.

Khanlari, G., Rafiei, B., and Abdilor, Y. (2015). Evaluation of strength anisotropy and failure modes of laminated sandstones. *Arabian Journal of Geosciences*. 8(5): 3089-3102.

Li, D., and Wong, L. N. Y. (2013). The Brazilian Disc Test for Rock Mechanics Applications: Review and New Insights. Rock Mechanics and Rock Engineering. 46(2): 269-287.

Liao, J. J., Yang, M. T., and Hsieh, H. Y. (1997). Direct tensile behavior of a transversely isotropic rock. *International Journal of Rock Mechanics and Mining Sciences*. 34(5): 837-849.

Ma, C.-C., and Hung, K.-M. (2008). Exact full-field analysis of strain and displacement for circular disks subjected to partially distributed compressions. *International Journal of Mechanical Sciences*. 50(2): 275-292.

Ma, T., Peng, N., Zhu, Z., Zhang, Q., Yang, C., and Zhao, J. (2018). Brazilian tensile strength of anisotropic rocks: review and new insights. *Energies*. 11(2): 304.

Markides, C. F., and Kourkoulis, S. K. (2012). The stress field in a standardized Brazilian disc: the influence of the loading type acting on the actual contact length. *Rock Mechanics and Rock Engineering*. 45(2): 145-158.

Niandou, H., Shao, J. F., Henry, J. P., and Fourmaintraux, D. (1997). Laboratory investigation of the mechanical behaviour of Tournemire shale. *International Journal of Rock Mechanics and Mining Sciences*. 34(1): 3-16.

Park, B., and Min, K.-B. (2015). Bonded-particle discrete element modeling of mechanical behavior of transversely isotropic rock. *International Journal of Rock Mechanics and Mining Sciences*. 76: 243-255.

Patel, S., and Martin, C. D. (2018). Evaluation of Tensile Young's Modulus and Poisson's Ratio of a Bi-modular Rock from the Displacement Measurements in a Brazilian Test. *Rock Mechanics and Rock Engineering*. 51(2): 361-373.

Ramamurthy, T. (1993). Strength and modulus responses of anisotropic rocks. *Comprehensive rock engineering*. 1(13): 313-329.

Rocscience (2016) RocFall 6.0 [Computer Software].

Singkhiaw, P., and Fuenkajorn, K. (2022). Effect of transverse isotropy on mechanical properties of Phu Phan sandstone. *In Proceedings of Acdemicsera International Conference (pp. 6-11).* Beijing, China.

Steen, B. V. D., Vervoort, A., and Napier, J. A. L. (2005). Observed and simulated fracture pattern in diametrically loaded discs of rock material. *International Journal of Fracture*. 131(1): 35-52.

Tan, X., Konietzky, H., Frühwirt, T., and Dan, D. Q. (2015). Brazilian Tests on Transversely Isotropic Rocks: Laboratory Testing and Numerical Simulations. *Rock Mechanics and Rock Engineering*. 48(4): 1341-1351.

Tavallali, A., and Vervoort, A. (2010). Effect of layer orientation on the failure of layered sandstone under Brazilian test conditions. *International Journal of Rock Mechanics and Mining Sciences*. 47(2): 313-322.

Tien, Y. M., Kuo, M. C., and Juang, C. H. (2006). An experimental investigation of the failure mechanism of simulated transversely isotropic rocks. *International journal of rock mechanics and mining sciences*. 43(8): 1163-1181.

Wu, Y., Li, X., He, J., and Zheng, B. (2016). Mechanical properties of longmaxi black organic-rich shale samples from south china under uniaxial and triaxial compression states. *Energies*. 9(12): 1088.

Yang, S.-Q., Yin, P.-F., Li, B., and Yang, D.-S. (2020). Behavior of transversely isotropic shale observed in triaxial tests and Brazilian disc tests. *International Journal of Rock Mechanics and Mining Sciences*. 133: 104435.

You, S., Sun, J., and Wang, H. (2021). Bedding Plane Effects on Mechanical Behavior of Surrounding Rock in Mountain Tunneling. *Shock and Vibration*. 1-10.

Yun-Si, L., Quan, Y., and Xiao, Z. (2012). The five elastic parameters for the anisotropy of slate under the influence of different bedding orientations. *Electronic Journal of Geotechnical Engineering*. 17: 3695-3707.

Zhang, X. J., Deng, H. F., Zhang, H. B., Wang, C. J., Fang, J. C., Xiao, Y., and Hu, Y. (2016). The influence of bedding angle on the tensile strength and failure mode of bedded sandstone. *Electronic Journal of Geotechnical Engineering*. 21(17): 5547-5558.

Zhu, W. C., and Tang, C. A. (2006). Numerical simulation of Brazilian disk rock failure under static and dynamic loading. *International Journal of Rock Mechanics and Mining Sciences*. 43(2): 236-252.
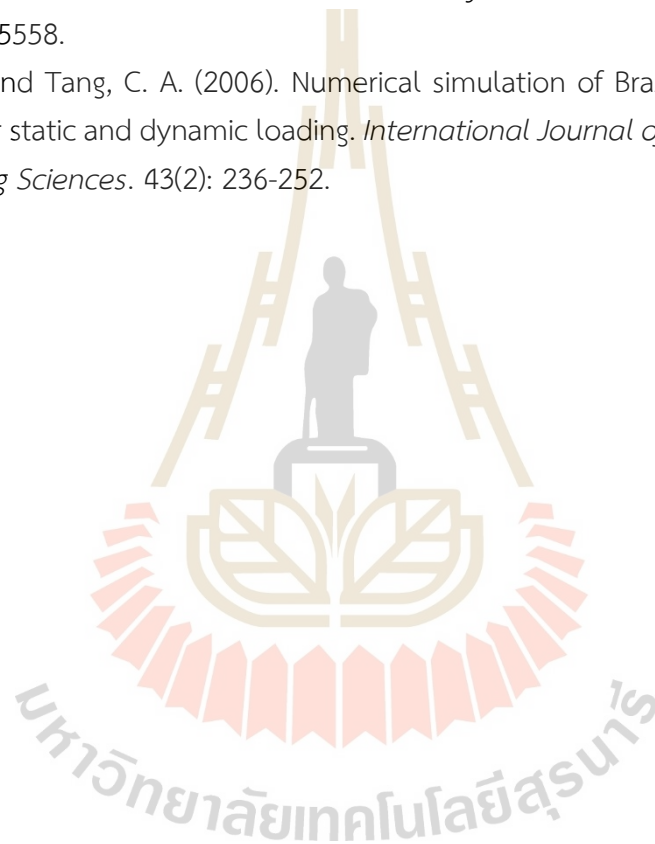
BIOGRAPHY

Miss Sawarot Suwankeeree was born on October 23, 1995 in Phichit Province, Thailand. She received her Bachelor's Degree in in Engineering (Geological Engineering) from Suranaree University of Technology in 2017. For her post-graduate, she continued to study with a Master's degree in Civil, Transportation and Geo-resources Engineering Program, Institute of Engineering, Suranaree University of Technology. During graduation, 2019-2022, she was a part time worker in position of teaching assistant at School of Geotechnology, Institute of Engineering, Suranaree University of Technology.